Spring 2018

Testing ^{10}Be Exposure Dating of Holocene Cirque Moraines using Glaciolacustrine Sediments in the Sierra Nevada, California

William Cary
Western Washington University, w.a.c.ary@gmail.com

Testing ^{10}Be Exposure Dating of Holocene Cirque Moraines using Glaciolacustrine Sediments in the Sierra Nevada, California

By

William Cary

Accepted in Partial Completion
Of the Requirements for the Degree
Master of Science

ADVISORY COMMITTEE

Dr. Douglas H. Clark, Chair

Dr. Robert J. Mitchell

Dr. Colin Amos

GRADUATE SCHOOL

Dr. Gautam Pillay, Dean

Master's Thesis

In presenting this thesis in partial fulfillment of the requirements for a master's degree at Western Washington University, I grant to Western Washington University the non-exclusive royalty-free right to archive, reproduce, distribute, and display the thesis in any and all forms, including electronic format, via any digital library mechanisms maintained by WWU.

I represent and warrant this is my original work, and does not infringe or violate any rights of others. I warrant that I have obtained written permissions from the owner of any third party copyrighted material included in these files.

I acknowledge that I retain ownership rights to the copyright of this work, including but not limited to the right to use all or part of this work in future works, such as articles or books.

Library users are granted permission for individual, research and non-commercial reproduction of this work for educational purposes only. Any further digital posting of this document requires specific permission from the author.

Any copying or publication of this thesis for commercial purposes, or for financial gain, is not allowed without my written permission.

William Cary

5/14/2018

Testing ^{10}Be Exposure Dating of Holocene Cirque Moraines using Glaciolacustrine Sediments in the Sierra Nevada, California

A Thesis
Presented to
The Faculty of
Western Washington University

In Partial Fulfillment
Of the Requirements for the Degree
Master of Science

By
William Cary
May 2018

Abstract

An ongoing study attempting to date boulders from Neoglacial moraines across the Sierra Nevada mountain range, CA using high precision cosmogenic radionuclide (CRN) exposure dating has yielded ages that contradict historical records and prior research in the range. The adjacent Lyell and Maclure glaciers in Yosemite National Park show remarkably different CRN age records, with the Lyell Glacier exhibiting ages consistent with late-Little Ice Age (LIA) formation and the Maclure Glacier displaying no late-LIA ages and several apparent clusters of ages at ~3.0, 2.3, and 1.0 ka. The Price moraines farther north show an even greater range of ages spanning the entire Holocene, with a distinct cluster at 2.7 ka and a marked absence of young ages. I collected glacial lake sediment cores from below each of these glacial systems to compare these CRN ages with an independent rock flour record constrained by radiocarbon, tephra, and ^{210}Pb dating. Using both these records I attempt to determine whether these clusters of CRN ages have glacial significance or are merely a function of geomorphic processes that promote inheritance. Apparent onset of Neoglaciation interpreted from rock flour deposition records from below the Lyell Glacier indicate glacial advances from ~1830-1230 cal yr BP with a peak at ~1790 cal yr BP and followed by another advance from ~610-80 cal yr BP with a peak at ~460 cal yr BP. The sediment core from Maclure Lake indicates rock flour deposition from ~1650-1280 cal yr BP and ~1020-370 cal yr BP with the apparent Holocene maximum ~970 cal yr BP. No rock flour record is apparent from the cores collected from Lake Aloha, below the Price cirque.

Based on historical accounts, prior research, and glaciolacustrine records from Lower Lyell Lake, I interpret CRN dating for the Lyell moraines represents true age of boulder emplacement on the moraine. The other two moraine sequences are more complex. I propose that the disparate CRN ages from the Maclure glacier are the result of an ice-cored moraine; ice-cored moraines can preserve exposure histories of numerous glacial advances by moraine reincorporation rather than obliteration. This hypothesis explains why CRN ages cluster within the Neoglacial period proposed by prior glaciolacustrine studies, as opposed to the Price moraines, and is consistent with moraine morphology. The Price CRN ages likely do

not represent glacial maxima because these older ages not only contradict historical records and prior glacial studies in the area, but also the striking youthful appearance of these moraine deposits. The Price CRN ages appear to be the result of inheritance, likely due to episodic rockfall events and reworked rocky debris versus subglacial plucking, evidenced by a lack of striations and/or polish on boulders and proximity to the steep cirque headwall. The Price glaciers were extremely small and likely lacked the erosive force to strip boulders of prior accumulated CRNs, making these deposits prone to inheritance issues even if a boulder had undergone several glacial advances. From these records, I suggest that larger glaciers with an ice-free core are better suited for this new, highly precise CRN exposure dating than smaller glaciers, or those with extensive ice-cored moraines.

Acknowledgements

This project was a huge undertaking and involved a great deal of effort from many people, institutions, and even mules. First and foremost, I would like to thank my advisor, Doug Clark, for continual support, guidance, and insight throughout the entirety of my time at WWU. His excitement for my research, and all his students' research, was contagious and helped motivate me during times of tedium. I also want to thank Doug for providing me with field sites and a project that inspired me. I am indebted to my numerous field assistants who, for perplexing reasons, decided to join in carrying heavy packs up thousands of feet and many miles without any form of compensation. These brave souls include Robin Thomas, Joe Morgan, Sam Schopler, Madison Swoy, Stephanie Truitt, and Darrell Lambert. Special thanks to Stephanie for loaning me her vehicle for fieldwork and to Darrell for backbreaking efforts. On that note, I should acknowledge the service that the Tuolumne Meadows Stables provided in hauling up ~410+ lbs. of equipment *most* of the way to the Yosemite field sites. I would be remiss without mentioning my gratitude for Hal Wershow, who provided me with insight, advice, and technical help with all the steps along the way. Many thanks to my committee members Robert Mitchell and Colin Amos for their insightful comments, edits, and fresh perspectives that improved this manuscript and the project overall.

This research would not have left the ground without Alan Hidy of LLNL being so willing to collaborate and share his CRN data. Thanks to Yosemite National Park and the Desolation Wilderness for granting me access to complete fieldwork in such stunning landscapes. Alex Hedgpeth was of enormous help while I processed my samples for radiocarbon dating and the whole staff at the CAMS facility at LLNL have my gratitude. Kanchan Maiti, from the Department of Oceanography and Coastal Sciences at Louisiana State University, generously processed my ^{210}Pb samples for in-house pricing. Elmira Wan, at the USGS Tephrochronology Project, fingerprinted the tephra samples. I want to acknowledge the immense help Ben Paulson was to me while completing lab work at WWU. I extend a big thanks to the Mobile of Lee Vining and Ski Run Liquor for accepting the odd request to store tubes of "mud" in their walk-in fridges for core preservation. This project was supported by the GSA Graduate Student Research Grant, Sigma Xi Grants-in-Aid of Research, LacCore and CSDCO Visiting Student Travel Grant, WWU RSP Fund for the Enhancement of Graduate Research, and WWU Geology Department Advance for Research.

Table of Contents

List of Tables

List of Figures

1.0 Introduction

Alpine glaciers are sensitive indicators of climate and associated climate changes (Meier, 1962); glaciers advance or retreat predominantly in response to changes in winter precipitation and summer ablation (Leonard, 1989). These glacial fluctuations effect local ecosystems, geology, and people. Temperate glaciers, like those in the Western Cordillera of the contiguous U.S., are often a dominant source of late-season cold water for local drainages (Fountain and Tangborn, 1985). Rapidly retreating glaciers can also produce geomorphic hazards including debris flows, mass failures of over-steepened valley walls, outburst floods from proglacial moraine lakes (Moore et al., 2009), and may even contribute to sea level rise (Meier et al., 2007). As such, it is crucial to understand how glaciers have fluctuated in the past in order to understand how they might respond in the future. Few studies provide records of glacier changes over the entire Holocene and, consequently, spatial and temporal Holocene variability in glaciers within the contiguous United States is not well-documented.

Two primary means of constraining glacial fluctuations that predate historical records are direct dating of moraines and indirect dating of glaciolacustrine sediment records down-valley of glacial deposits; each method has benefits and limitations. Moraines directly record periods of maximum advance and, therefore, cooling and/or increased winter precipitation. The vast majority of Holocene moraines within the contiguous Unites States terminate above treeline and cannot be dated by radiocarbon isotopes (e.g., Mood and Smith, 2015; Wiles et al., 2011). The advent of cosmogenic radionuclide (CRN) exposure dating enables direct dating of these Holocene moraines. This method offers a means of constraining patterns of such glacial advances across broad regions but is subject to significant uncertainties related to inheritance and/or post-depositional processes. Conversely, glaciolacustrine deposits provide continuous records of glacier activity in individual valleys, from initiation and growth to maxima and then retreat. However, glacial lake sediment records are indirect measures of glacial extent and activity and, therefore, are more difficult to interpret than moraines. They are also difficult to collect

and are typically viable only in exceptional locations, hindering testing of regional patterns of glacier activity.

In this study I compare CRN and glaciolacustrine geochronology data related to Holocene glacial activity of the Lyell and Maclure glaciers in Yosemite National Park, CA as well as for a set of small moraines on the slopes of Mt Price in the Desolation Wilderness (Figure 1). A primary motive for this study was to test the widely disparate ^{10}Be CRN exposure ages of boulders from geomorphically young moraines (interpreted as late-Little Ice Age – LIA) during an initial dating effort in the Sierra Nevada (Clark et al., 2015). In particular, boulder ages from moraines below the adjacent Lyell and Maclure glaciers displayed widely contrasting clustered ages despite their close proximity. To test the validity of these incongruous results, I collected three sets of glaciolacustrine cores from lakes directly below these moraines and below geomorphically similar moraines at Mt. Price to compare with the respective CRN dating records. The results suggest that CRN dating of moraines from such small cirque glaciers have significant uncertainties beyond those typically acknowledged (e.g., inheritance, moraine diffusion). Additionally, I propose several geomorphic processes that help resolve the asynchronous glacial fluctuations apparent from CRN dating, particularly that relate to the adjacent Lyell and Maclure glaciers.

2.0 Background

2.1 Geologic Setting

This study focuses on Holocene cirque glaciers in the Sierra Nevada of California, part of the Western North American Cordillera. Specific field locations include the moraines and lakes below the Lyell and Maclure glaciers in Yosemite National Park and below Mt Price near Lake Tahoe in the Desolation Wilderness. At each site, the cirques have steep north to northeast-facing headwalls that act as wind-traps for winter snow accumulation and provide sun shielding during the summer, reducing ice ablation. Bedrock of the Maclure and Lyell field sites consists of granodiorite, metavolcanic rock, diorite,

and gabbro (Huber et al., 2003). Bedrock of the Price field site comprises granodiorite, diorite, gabbro, and granite (Saucedo et al., 2005). These high-alpine regions in the Sierra Nevada have been extensively scoured by multiple generations of glaciation throughout the Pleistocene (known in the Sierra Nevada as the Tahoe, Tenaya, Tioga, Recess Peak glacial advances) (Sharp and Birman, 1963; Clark and Gillespie, 1997; Phillips et al., 2009; Rood et al., 2011), such that the field sites near the Holocene moraines are predominantly stripped, relatively fresh, and often polished bedrock. The Holocene moraines at each field site are characterized by steep, unstable slopes, a lack of vegetation (even lichen in many cases), and sharp, well-defined contacts with surrounding bedrock; these features indicate a very young age of deposition (Figure 2).

The target lakes associated with these glaciers are well suited for lake sediment core analysis because they are all bedrock dammed, directly fed by outwash from the cirque glaciers, and are immediately down-slope of the mapped Neoglacial maxima at each site (Figures 3 & 4). Furthermore, because the basins are dominated by stripped granitic bedrock, there are few non-glacial sources for fine clastic sedimentation that is a primary proxy for glacial activity upstream. Consequently, these lakes should have captured continuous sedimentation (glacial rock flour) from glacial advances and retreats throughout the entire Holocene (e.g., Bowerman and Clark, 2011).

2.2 Post-LGM Climate and Glacial fluctuations of the western North American Cordilleran

Mountain glaciers throughout most of the American Cordillera reached their late-Pleistocene maxima during Oxygen Isotope Stage 2 (~25-18 ka), after which most experienced rapid retreat and largely disappeared in most regions by ~15-16 ka (Margold et al., 2014; Riedel et al., 2010; Brugger, 2007; Guido et al., 2007; Licciardi et al., 2004; Briner et al., 2005; Rood et al., 2011). Following a short interval of warmer and drier conditions, portions of the highest mountains experienced a brief period of glacier advance during or immediately before the European Younger Dryas period (Clark and Gillespie, 1997; Davis et al., 2009; Menounos et al., 2009; Osborn et al., 2012). In the Sierra Nevada, this event is

termed the Recess Peak advance and ended before ~13,100±85 cal. years BP (Clark and Gillespie, 1997), shortly before the beginning of the Holocene at 11.7 ka. In most regions, including the Sierra Nevada, these latest Pleistocene advances extended beyond any subsequent Holocene advances (Clark and Gillespie, 1997; Davis et al., 2009) and, thus, provide a distinct limit on extent of any Neoglacial activity.

Globally, the early Holocene (~11.0-5.0 ka) was characterized by relatively warm conditions followed by overall cooling of ~0.7°C through the middle to late Holocene, which culminated in the LIA of the last Millennium (Marcott et al., 2013). Glaciers in the North American Cordillera appear to have responded to these shifts in temperatures through a series of advances and retreats. Alaskan glaciers advanced at about 4.5-4.0, 3.3-2.9, 2.2-2.0, 1.4-1.2 ka and then with progressively larger advances during the last millennium at 1180-1320, 1540-1710 and 1810-1880 CE (broadly encompassing the extent of the LIA); these advances were dated using radiocarbon and tree-ring dating of wood collected in glacier forfields and moraines, glaciolacustrine records, lichenometry and CRN dating of moraines (Calkin et al., 2001; Wiles et al., 2002; Barclay et al., 2009; Wiles et al., 2011; Solomina et al., 2015). Glaciers in western Canada were the least extensive in the early Holocene from ~11-7 ka with advances, documented by radiocarbon ages from wood collected from glacier forfields, occurring at ~8.6-8.2, ~7.4-6.5, ~4.4-4.0, ~3.5-2.8, ~1.7-1.3 ka and the past millennium (Menounos et al., 2009). Mood and Smith (2015) document similar timings of glacial fluctuations in the British Columbia Coast Mountains, with the addition of one advance from 5.4-5.3 ka, based on overridden wood samples in glacier forfields, sediment cores, and lichenometry. Neoglacial advances on Mt Baker in the North Cascades, documented by tephra and radiocarbon dating of stacked tills along the right lateral moraine of the Deming Glacier, occurred at ~6.0 ka, ~2.2 ka, ~1.6 ka, ~0.9 ka, ~0.4 ka, reaching maxima late in the LIA in the mid-1800s (Osborn et al., 2012). In most accounts these Holocene advances are characterized by successively larger glacial extents, peaking during the height of the LIA (~18th & 19th centuries). Since the end of the LIA (~200 yrs BP), global temperatures have increased and are now warmer than during ~75% of the Holocene (Marcott et al., 2013).

Most moraine evidence of early Neoglacial activity in the U.S. Cordillera prior to the late-LIA has been over-ridden and obliterated, obscuring the terrestrial Neoglacial record in many ranges. Additionally, because these glaciers predominantly terminated above the treeline (in contrast to those in Alaska, Canada, and the larger Cascade volcanoes), these deposits contain little or no datable organic material associated with their timing of formation. Accordingly, alternative methods must be employed to date moraines and discern longer-term histories (pre-LIA maximum), primarily CRN dating and glaciolacustrine proxy records.

2.2.1 Sierra Nevada Glacial Record

Early studies documented the activity and extent of glaciers in the Sierra Nevada. John Muir (1875) first documented "living glaciers" in the range in 1871 by recording flow rates using a series of surveyed stakes on the Maclure Glacier in 1872. The first glacier map in the Sierra Nevada, of the Lyell and Maclure glaciers (Figure 5; Russell, 1889), indicates that both glaciers were at or near their Holocene maximum positions in 1883. Of note on this map is that the Maclure Glacier extent is depicted to be much farther down than the moraines indicate, terminating with a calving front in Maclure Lake. For this reason, it is questionable if this map accurately portrays true glacier extent or, rather, residual snowfall. More recent studies (Basagic, 2008; Basagic and Fountain, 2011) compare these early studies with subsequent historical observations to document a consistent overall decrease in glacial extent from the first observations to the present.

Stock et al. (2013) recently measured flow rates over four years (2009-2012) of both the Lyell and Maclure glaciers in Yosemite National Park. Their measurements showed no detectable movement at the Lyell Glacier, indicating that the glacier had stagnated by 2012. Despite a significant decrease in size, the Maclure Glacier is still flowing at about 7.2 meters per year, the same rate John Muir measured in 1872. The dominant mode of movement for the Maclure Glacier may have shifted from internal deformation to basal sliding because the glacier is melting more rapidly and has less volume and, thus,

less mass to cause deformation (Stock and Anderson, 2012). The small moraine deposits near Mt Price all lie below cirques that are now ice-free, but have been correlated geomorphically to be of similar age to the LIA deposits in Yosemite (Clark and Gillespie, 1997). In addition, historical accounts of small glaciers occupying the cirques have been reported (Whiting, 1985).

Glacial fluctuations during the Holocene in the Sierra Nevada appear to follow a similar, although abbreviated, pattern to glaciers in the mountain ranges farther north. Following the retreat of the late-glacial Recess Peak glaciers (~12,000 cal yr BP), the Sierra Nevada appears to have remained essentially unglaciated until the late Holocene (Clark and Gillespie, 1997; Phillips et al., 2009). Based on the rock flour record below the Palisade Glacier (Bowerman and Clark, 2011) and the Conness Glacier (Konrad and Clark, 1998), glacial maxima of progressively larger extents were interpreted at ~3200, ~2200, ~1600, ~700, and ~250-170 cal yr BP. The most recent advance (Matthes in the Sierra Nevada, traditionally regarded as late-LIA) has been considered the most extensive Neoglacial advance and, by inference, obliterated geomorphic evidence of previous Neoglacial advances. Wood (1977) also support the LIA designation for the Matthes advance in the Ritter Range, just south of the Lyell and Maclure glaciers, documenting a distinct absence of a Mono tephra ("Tephra 1") that mantles all other moraines in the range. Accordingly, Wood (1977) concluded that these moraines could not be older than 720±60 B.P. Still, this interpretation is based on local records of a few glaciers and geomorphic correlation of mapped moraine extents. Inferring regional significance and glacial fluctuations for the entire Sierra Nevada from these two dated sites and moraine correlations may be problematic, especially considering these new CRN ages.

2.3 Glaciolacustrine Records

As glaciers grow the net glacial abrasion of bedrock increases due to larger affected surface area and generally higher flow rates. This abrasion in turn increases the flux of glacial rock flour, fine-grained suspended rock powder, into downstream proglacial lakes where it gradually settles onto the lake bottom (Karlén, 1981; Dahl et al., 2003). Conversely, as glaciers shrink, rock flour production and deposition will decrease. These changes in rock flour production are recorded in pro-glacial lake sediment stratigraphy (Karlén, 1981; Leonard, 1985). Such sediment records can thus yield continuous records of glaciation upstream in a basin. Rock flour sedimentation rates may remain relatively high with respect to ice extent for up to the first century after ice decline due to unstable glaciogenic deposits being exposed to runoff and fluvial processes during ice recession; this process may create a lag of peak rock flour deposition in the glaciolacustrine record with respect to the glacier mass-balance (Leonard, 1986). In the Sierra Nevada, however, Bowerman and Clark (2011) concluded that the small, boulder-dominated moraines typical of Holocene deposits in the range do not appear to exhibit the same lag effect.

Proglacial lakes in the Sierra Nevada provide excellent sites for recording changes in glacial rock flour production. The glacially stripped granitic cirque basins typical of the range have only a few primary sources of clastic sediment: rock flour (if a glacier is present), slope-wash, stream bedload, aeolian dust, and volcanic tephra. In contrast to the fine silt size of rock flour, slope wash and bedload in Sierra Nevada basins are generally dominated by sand-sized gruss and larger sediments (Bowerman and Clark, 2011). Additionally, aeolian dust, although similar in size to rock flour, is generally more weathered, brown in color due to higher organic content and oxidized clastics, and less magnetic, thus having a weaker magnetic susceptibility (MS) signal (Snowball, 1993; Matthews et al., 2000; Rosenbaum et al., 2012). Rock flour is typically blue-grey in color, which is reflected in the visual stratigraphy of glaciolacustrine sediments (Dahl et al., 2003). During times of increased glacial activity, the rock flour signal inundates the organic signal, which is reflected by a coincident decrease in Loss on Ignition (LOI) (Karlén, 1981; Matthews et al., 2000; Dahl et al., 2003; Bakke et al., 2005). Volcanic tephra is readily

distinguished from rock flour in the Sierra Nevada by their light grey color and presence of glass shards in petrographic analysis.

Several different methods provide age control to core records. Terrestrial macrofossils and/or organic rich sediment are often present, having been deposited and incorporated into the lake sediments, providing a means to date interpreted glacial maxima using radiocarbon dating (e.g., Clark and Gillespie, 1997; Konrad and Clark, 1998; Bowerman and Clark, 2011). Caution should be used with bulk radiocarbon dates of organic sediment, though, which have been shown to lag the true age by up to 2000 years in some settings (Grimm et al., 2009; Bertrand et al., 2012). This reservoir effect, however, may not be significant in high alpine Sierra Nevada environments. There are no sources of inorganic carbon from bedrock in the study drainages. Furthermore, Clark and Gillespie (1997) tested the reservoir potential in Sierran alpine lakes with paired radiocarbon dates of bulk organic gyttja and adjoining terrestrial macrofossils. Of four paired dates, only one date showed any significant reservoir effect in the bulk sample. Additionally, ^{210}Pb dating of the uppermost sediments and volcanic tephra fingerprinting can add further age constraints (e.g., Bowerman and Clark, 2011; Wershow, 2016). With these ages, sedimentation rates are determined to constrain the timing of glacial activity.

2.4 Cosmogenic Radionuclide Exposure Dating

Earth is continually bombarded by cosmic radiation, some of which reaches the Earth's surface where it is progressively absorbed within the upper few meters of rock or regolith and interacts with specific elements in rocks to produce several rare cosmogenic radionuclide isotopes, or CRNs (Cockburn and Summerfield, 2004). By analyzing the concentrations of CRNs in rocks, and the rates at which they are produced, timing and rates of various geomorphic processes or events can be quantified (Gosse and Phillips, 2001). In terms of dating, CRN concentrations are used to estimate the time elapsed since a rock was exposed at the surface. Although CRN dating can be a useful method to determine moraine boulder emplacement, reliable exposure ages require several key assumptions. (1) The sampled surface must have

originated several meters below the original surface (below the cosmic ray penetration depth) and been exhumed rapidly (Ivy-Ochs et al., 2007). (2) The surface should have been exposed to cosmic rays continuously since exhumation without significant snow cover, burial, or erosion (Hallet and Putkonen, 1994; Putkonen and Swanson, 2003; Kirkbride and Winkler, 2012). (3) The surface should have remained stable since exposure without post-depositional disturbance (Hallet and Putkonen, 1994; Briner et al., 2005). Any deviations from these assumptions will contribute scatter to the model exposure ages of the deposit of interest, where exposure ages appear either older than the actual deposition age due to inheritance or younger due to post-depositional modification of the surface or shielding of the surface from burial (e.g., snow, sediment, or vegetation cover).

^{10}Be CRN analysis of boulders is now a well-established method for dating Pleistocene moraines (e.g., Licciardi et al., 2004; Brugger, 2007; Schaefer et al., 2009; Putnam et al., 2013; Doughty et al., 2015; Schaefer et al., 2015). Until recently, however, the analytical uncertainties were too large to reliably date boulder emplacement in Holocene deposits. Recent advances in analytic methods at a few labs have enabled precise ^{10}Be exposure dating of boulders as young as late-LIA (Zimmerman, 2014). An ongoing study led by Susan Zimmerman and Alan Hidy from the Center for Accelerator Mass Spectrometry (CAMS) at Lawrence Livermore National Laboratory (LLNL) is using CRN dating on boulders emplaced on small Holocene cirque moraines in the Sierra Nevada, CA. The preliminary results from this study have yielded some unexpected findings; whereas some moraines have boulder ages that are largely consistent with late-LIA formation (~200-350 yr B.P.), other moraines have clusters of ages that are all thousands of years older (Figures 6 & 7) (Clark et al., 2015). The CRN ages from boulders along the Lyell moraines nearly all fit within the late-LIA (Figure 8) while the CRN ages from Maclure moraine boulders exhibit clusters at ~3.0, 2.3, and 1.0 ka with the youngest age at ~0.6 ka (Figure 9). The boulders from the Price deposits are even more varied, with clusters at ~10.5, 7.7, 5.6, and 2.7 ka (Figure 10). No LIA ages are present in the Price CRN ages.

This wide spread of moraine exposure ages conflicts with previous studies of Holocene glaciation in the range based on historical records, geomorphic mapping, and lake sediment coring, which all

indicate that maximum Holocene glacial extents occurred during the late-LIA (Wood, 1977; Konrad and Clark, 1998; Bowerman and Clark, 2011). Although inheritance (prior exposure of rocks in the cirque headwalls) may account for some of the pre-LIA boulder ages, this explanation is inconsistent with both the groupings of older ages, and with the absence of any LIA ages in several of these deposits. Alternative explanations are that the ages are accurate and Holocene glaciation in the Sierra Nevada was far more complex than previously thought, or that other largely unrecognized processes affect moraine formation on these cirque glaciers (e.g., periglacial activity, episodic rockfall events, debris cover, and/or ice-cored moraine development).

3.0 Methods

3.1 Site Selection

In this study, I selected three glaciated cirques in two field areas located in the Sierra Nevada to test the contrasting explanations described above for the disparities in CRN exposure ages relative to previous interpretations of Holocene moraine formation (Figure 1). The sites have several characteristics that make them well suited for this study: the Holocene moraines are distinct and geomorphically well defined. There are no prior glaciolacustrine records at the sites and the proglacial lakes are well-situated down-valley of the maximum Neoglacial extent as to record complete sediment records from each cirque. The granitic basins have been extensively stripped by Pleistocene glaciation, reducing possible non-glacial sources for fine clastic sediments. The Yosemite field sites (Lyell and Maclure) exhibit two distinct moraine records according to preliminary ^{10}Be ages despite being directly adjacent glaciers, so the potential local variability of glacier activity can be directly tested. Additionally, the Desolation field site is the northernmost location of mapped Neoglacial moraines in the Sierra Nevada (Clark, 1995), so I can test the regional variability of glacier responses. All sites are accessible by trail and pack mules were available in Yosemite to aid with equipment transport.

3.2 Remote Mapping

To establish the Holocene glacial context of each site, I mapped both modern and maximum Neoglacial extents. Mapping of both these glacier extents at each target site was completed using lidar imagery (2007-Yosemite NP) and georeferenced Google Earth imagery (2013-Yosemite NP, 2012-Desolation) in ArcGIS 10.3.1. For this study, I consider "modern" to be 2013 in Yosemite and 2012 in the Desolation Wilderness because these are the dates of the most recent low-snow imagery available. This ensures that the imagery depicts actual glacial extents versus residual winter snow. Surface areas of the glaciers were calculated for each extent of each respective glacier. Additionally, I mapped local watersheds for the target lakes below the Lyell and Maclure glaciers using a pour-point method in ArcGIS 10.3.1 based on the 2007 lidar data.

3.3 Lake Sediment Coring

3.3.1 Bathymetry

The deepest portions of lake basins usually provide the highest resolution and most complete sediment records (Larsen et al., 1998). I collected detailed bathymetric data of all potential lake coring sites below the Lyell, Maclure, and Price glaciers (Figures 3-4). For each lake, I recorded depth data along a systematic grid in portable inflatable rafts, taking GPS points every ~10-25 meters, using the Trimble GeoXH 6000, and recording the water depth using a handheld bathymetry meter. In the lab, the GPS data were differentially corrected (most uncertainties were < 1m). In Surfer 8, the GPS data were compiled and used to create detailed bathymetry maps.

3.3.2 Lake Sediment Coring

Specific coring locations at each field site were selected based on lake bathymetry, distance from actively forming deltas at lake inlets, distance from steep slopes that may disrupt sediment stratigraphy by mass movements (e.g., rockfall, slumps, etc.), and anchoring limitations while in the field. Because of anchoring difficulties in Maclure Lake, coring was completed in the shallowest portion of the bottom shelf farthest from the inlet. Coring in Lake Aloha was moved ~30 m NW of the deepest portion of target basin to avoid possible coarse sediment from the adjacent steep talus to the west.

To recover the poorly consolidated uppermost sediments, I used a Glew corer (Glew, 1991). This system is a single-push gravity and percussion system. Each Glew core was analyzed for MS in the field; all but one core from Lake Aloha were then sub-sampled in the field into plastic sample bags in 1 cm increments corresponding to the MS measurements. The remaining Glew core from Lake Aloha was drained of excessive water and treated with Zorbitrol, a sodium polyacrylate absorbent powder, to solidify the remaining water and stabilize the uppermost, poorly consolidated sediments for transport out of the field. For deeper sediments from Lower Lyell Lake and Maclure Lake, I collected cores using a 2 in (50.8 mm) diameter modified Livingston piston corer (Wright Jr., 1967). After collection, the cores were extruded in the field into split PVC pipes, measured for MS at 2-cm increments using a Bartington MS2-C logger, and transported to the lab.

3.4 Core Analysis

3.4.1 Sediment Analyses

Detailed and high-resolution analysis of core stratigraphy is critical to establish the timing and magnitude of the glacial rock flour signal and to differentiate it from other non-glacial components such as organic matter, slope-wash, and tephra. I completed the Initial Core Description (ICD) process at the LacCore facility at the University of Minnesota following their standard protocols (Myrbo, 2005). Whole core multisensory logging using a GeoTek Multi-Sensor Core Logger (MSCL) provided MS, P-wave velocity, gamma density, and electrical resistivity data. Cores were then split, and the surfaces prepared

with a rounded glass slide. High-resolution imagery of each prepared core was captured with a Geotek Geoscan-III. Higher resolution MS data were collected using a Bartington MS2E point sensor for split cores (0.5 cm intervals) and bagged Glew core sediments. I logged visual stratigraphy based on color, clast size, lithology, and organic content as well as noting the nature of boundaries between stratigraphic layers. I also made smear slides for each distinct stratigraphic layer to assess the sediment for tephra, diatoms, organic content, and clastic content.

Further core analyses were conducted in the Sediment Coring Lab at WWU, including LOI and laser particle size analysis. Samples for each analysis were extracted at uniform depths using a 1 cm^3 syringe at 2 cm intervals; occasionally the sampling interval was adjusted to capture different stratigraphic layers throughout the core. LOI samples were desiccated at 100 °C overnight, weighed, burned for 4 hours at 550 °C to remove organic matter, and weighed again. LOI was calculated as a percentage using the following formula:

$$LOI(\%) = \frac{(W_{dry} - W_{burn})}{W_{dry}} \times 100 \quad (1)$$

where W_{dry} = desiccated weight and W_{burn} = weight after burn. Grain size distribution samples were pretreated with a 30% hydrogen peroxide solution in a heated, sonicated bath to remove organic matter that is not representative of clastic sedimentation. Diatoms, observed in smear slides, were subsequently removed using a 1M NaOH solution. NaOH reactions were neutralized with a 0.5 N HCL solution to mitigate clastic silica digestion. Laser particle size samples were analyzed using a Malvern Mastersizer 2000 with autostage and exported into the following grain size ranges: clay = <3.9 μm, fine silt = from 3.9 - 15.6 μm, coarse silt = from 15.6-62.5 μm, fine sand = from 62.5 – 250 μm, coarse sand from 250 – 2000 μm.

3.4.3 Sediment Dating and Age-Depth Modeling

Sediment core chronologies were developed using ^{210}Pb dating, tephrochronology, and Accelerator Mass Spectrometry (AMS) radiocarbon dating. The uppermost sediments of sampled Glew cores were dried, ground to a uniform size, weighed, and sent to the Department of Oceanography and Coastal Sciences at Louisiana State University for ^{210}Pb analysis. Tephra deposits were fingerprinted using electron microprobe analysis of nine major and minor oxides (SiO_2, Al_2O_3, FeO, MgO, MnO, CaO, TiO_2, Na_2O, K_2O) by the USGS Tephrochronology Project Laboratory in Menlo Park, CA. For radiocarbon dating, a lack of identifiable terrestrial macrofossils in the cores required us to rely on bulk organic sediments. The samples were analyzed at the CAMS facility at Lawrence Livermore National Laboratory. Radiocarbon ages were calibrated using the IntCal13.14c curve and CALIB version 7.10 (Stuiver and Reimer, 1993).

I performed age-depth modeling using *Bacon* (Bayesian Accumulation), an R-based statistical model that provides uncertainty based on input ages (Blaauw and Christen, 2011). The model divides cores into vertical intervals and runs millions of Markov Chain Monte Carlo iterations to estimate the sedimentation rate and generate an associated date for each cm depth. I set the section thickness to 3 cm for the Lyell core and 2 cm for the Maclure core to increase resolution and smooth the output. Age constraints were entered as both uncalibrated for radiocarbon ages and calibrated for ^{210}Pb and tephra ages. Radiocarbon ages were automatically calibrated in *Bacon* using the IntCal13.14c curve. Additionally, I changed the default memory setting from 0.7 to 0.3, the lowest memory setting, to reflect more variability within the core and calculate sedimentation rates for each interval with little influence from surrounding intervals. All other parameters operated under default settings.

Tephra intervals were not removed from core stratigraphy for determining sedimentation rates due to negligible impact on this study. If tephra is removed from the Lyell stratigraphy to account for instantaneous deposition, there would be a ~1.4% decrease from 22-44 cm depth and ~4.5% decrease from 44-132 cm in sedimentation rate. Maclure has only one tephra layer and removal of this 0.5 cm thick

tephra results in a ~1.3% decrease in sedimentation rate between 25-65 cm depth. All other sedimentation rates remain constant.

3.4 CRN Exposure Dating Analysis

I used the reduced chi-squared (χ_R^2) statistic as described in Balco (2011) to determine the degree of geologic scatter for groups of CRN ages:

$$\chi_R^2 = \frac{1}{n-1}\sum_{i=1}^{n}\left[\frac{t_i - \overline{t_i}}{\sigma t_i}\right]^2 \quad (2)$$

Where n is the number of ages, t_i are each individual CRN age, $\overline{t_i}$ is their mean, and σt_i are the respective uncertainties. This statistical test is a method of determining whether a certain set of ages contains variance due to geologic processes (i.e., inheritance or post-depositional processes) or analytic uncertainty. If the χ_R^2 value is ~1, scatter is explained entirely by measurement uncertainty. Moraine data sets with $\chi_R^2 = \sim 1$ can thus be averaged to determine an accurate age for moraine formation.

4.0 Results

4.1 Mapping Glacial Lake Watersheds

The watershed for the cored Lower Lyell Lake in Yosemite is ~1.14 km^2 and the Maclure Lake watershed is ~1.39 km^2. The Neoglacial terminal moraine for the western lobe of the Lyell glacier encompasses two drainages that flow to both the cored lake as well as the basin associated with the eastern lobe of Lyell glacier (Figure 11). Accordingly, the Lyell glaciolacustrine core only records sedimentation for the western portion of the western lobe of Lyell Glacier during the Neoglacial maximum. So, the lake core does not record glacial activity for the remainder of the glacier, which encompasses all CRN ages except LyellWB samples. The Maclure Lake watershed is relatively simple in comparison, encompassing the entire Maclure Glacier.

4.2 Core Recovery

I collected sediment cores from each target lake below the Lyell and Maclure glaciers, as well as the Price cirque moraines in August of 2016 (Figures 12, 13, & 14). At Lower Lyell Lake, I recovered one 1.54 m long Livingston core, comprising four separate pushes, from the depocenter at 5.0 m water depth. I also recovered 32 cm of the uppermost sediments using the Glew corer from Lower Lyell Lake. From the Maclure Lake, I recovered 2 adjacent Livingston cores from water depths of 8.8 m: a single-push 95-cm long core and a two-push 96-cm long core. The single push core is continuous and was better preserved following extrusion, so I focus my interpretations on this core. Additionally, I retrieved a 35 cm Glew core of the uppermost sediments in Maclure Lake. Two Glew cores were recovered from Lake Aloha in the Desolation Wilderness. The first core collected was 51 cm long and the second was 47 cm long at water depths of 12.4 m and 11.9 m respectively. The second core bottomed into a tephra deposit that was greater than 8 cm thick.

4.3 Sediment Stratigraphy

4.3.2 Lyell Cores

Sediment cores from Lower Lyell Lake are composed of distinct intervals of dark brown-higher organic sediments, light tan siliciclastic sediments, tephra intervals, and coarse sandy intervals (Figure 15). The lower 110 cm of the Lyell core exhibit low MS values between ~0-30 $m^3/kg \cdot 10^{-8}$. In this interval, sediment is a dark brown color and LOI is relatively high (~8-13%) except for four tephra intervals and a coarse sandy interval centered at 68 cm depth where LOI is <5%. At 42 cm depth the MS values rise sharply to ~85 $m^3/kg \cdot 10^{-8}$ and LOI drops below 5%, coinciding with a thin tephra layer and a thicker siliciclastic layer from 42-20 cm depth. As the siliciclastic interval grades up into darker brown sediment, the MS drops to ~25 $m^3/kg \cdot 10^{-8}$. Average LOI remains below 5% through the top 42 cm of the core. At ~10 cm depth there is another small increase in MS to 35 $m^3/kg \cdot 10^{-8}$ before dropping to 0 at the top of the core.

Grain size distribution remains stable from the bottom 110 cm of the core; exceptions are related to tephra intervals and a single coarse sandy interval at 68 cm depth (Figure 16). From ~42 cm depth to the top of the core, clay, fine silt, coarse silt, and fine sand percentages are more variable. Clay, fine silt, and coarse silt all trend into lower overall percentages of the grain size distribution in the top 42 cm. During the most prominent portion of the siliciclastic interval from 42-20 cm depth, however, there is a distinct peak in fine-grained silt that exceeds all other measured values throughout the core. Fine sand increases through the top 42 cm and coarse sand makes up a very small component of grain size distribution other than a thick coarse sandy interval centered around 16 cm depth.

4.3.3 Maclure Cores

Sediments from Maclure Lake contrast markedly with those in the adjacent Lower Lyell Lake. The cores contain predominantly coarse sandy gruss separated by substantial fine-grained intervals (Figure 17). The fine-grained intervals dominate between ~95-62 cm and 28-8 cm depth. Coarse sandy layers correspond to extremely low LOI values (≤2%) and to relatively low percentages of clay, fine silt, coarse silt, and fine sand (Figure 18). Conversely, silt percentages increase during finer grained intervals. LOI also increases during fine-grained intervals but remain below 5%. There are two main intervals of high MS values (>~100 $m^3/kg \cdot 10^{-8}$) located from 82-60 cm and 26-4 cm depth. These two peaks in MS generally correlate to the two intervals dominated by fine-grained sediment. The fine-grained intervals from the core bottom to ~60 cm depth contain a higher proportion of diatoms than the fine-grained intervals near the top of the core. One distinct tephra layer, ~0.3 cm thick, is located at 43 cm depth. In the top 41 cm of the Maclure core, there are several intervals of unusual red/green staining that affect mainly coarse-grained sediment except for at ~28-23 cm depth where some finer grains are also stained.

4.3.1 Lake Aloha Cores

Sediment cores from Lake Aloha below the Price glaciers are composed primarily of dark brown gyttja. LOI averaged ~ 20% indicating relatively high levels of organic material except for the thick basal tephra layer that was <10% organic content (Figure 19). Unfortunately, the basal tephra layer liquefied partially during transport to the lab and shifted upward ~10 cm. Therefore, I disregard the sediments below this level (~25-cm sediment depth). Sediments above this level, however, do not show signs of disturbance and so appear to remain intact. MS values are low, <5 $m^3/kg \cdot 10^{-8}$, throughout the core above the disturbed tephra layer, below which MS rises to ~13 $m^3/kg \cdot 10^{-8}$. Grain size distribution is relatively consistent throughout the undisturbed portion of the core with a slight decrease in clay, fine silt, and coarse silt and a corresponding increase in fine and coarse sand centered around 4 cm depth (Figure

20). There are mica grains throughout the core, but this shift in grain size distribution coincides with a significant increase in concentration of mica grains as seen in the visual stratigraphy.

4.4 Lake Sediment Chronology

4.4.1 Age Constraints

I analyzed five bulk radiocarbon samples, two samples from the Lyell core and three from the Maclure core (Table 1). Sample LM16-C-03, at 92 cm depth near the base of the Maclure core, records an age of 5830-5755 cal yr BP, indicating the Maclure record extends to mid-Holocene. The four other radiocarbon dates were positioned to constrain the interpreted glacial rock flour intervals. ^{210}Pb analysis shows unsupported ^{210}Pb for the top 4.5 cm in LL16-G01 and the uppermost 2 cm in LM16-G01. Sediment ages were calculated assuming a constant supply of unsupported ^{210}Pb to the sediment (Appleby and Oldfield, 1978). ^{210}Pb is an isotope produced through the ^{238}U decay sequence. In sediments and soils, there is a constant production and decay of ^{210}Pb that reaches equilibrium, resulting in a low-level, supported concentration throughout sediment or soil cores. Unsupported ^{210}Pb is produced in the atmosphere, subsequently raining out and incorporated only into the uppermost sediments, resulting in a decrease in concentration down the core (Appleby and Oldfield, 1978). From ^{210}Pb, the calculated sediment accumulation rate for LL16-G01 is 0.27±0.003 mm/yr, or 2.7±0.3 cm for the past 100 years. For LM16-G01, the sediment accumulation rate was 0.077±0.003 mm/yr, or 0.77±0.3 cm over the past 100 years.

Three tephra samples, LL16-T-01, LL16-T-02, and LM16-T-01, were fingerprinted to add age constraints to the Lower Lyell Lake core and the Maclure Lake core (Table 2). LL16-T-01 and LL16-T-02 identified as early Holocene Mono tephras with an age range of ~2.0-0.8 ka. These ages align with bulk radiocarbon dates for the Lyell core, but not completely with the Maclure core where the younger age range would not align with bulk radiocarbon ages. Regardless, the range is too large to be incorporated into the sedimentation model because I do not know the specific eruptions from which these

tephras were generated. Thus, neither were used for the respective age-depth models. It is important to note, however, that if LM16-T-01 is from a younger eruption, it would shift the age model and indicate a reservoir effect for the bulk radiocarbon samples. The analysis of LL16-T-02, from 136 cm sediment depth in the lower Lyell core, was polymodal with three geochemical populations. The major population, 23 shards, was identified as the Tsoyowata ash, which erupted from Mt Mazama ~7.74-7.95 cal kyr BP (Bacon, 1983). The intermediate subpopulation, 9 shards, was another cascade type tephra that originated from Crater Lake but does not have an age of eruption. The minor population, 4 shards, was identified as reworked late and early Holocene Mono Craters tephra. It is common for tephra samples to be polymodal due to reworking in the depositional environment or coring / extrusion disruption of the perimeter in cores with multiple tephras present. In this case, the relatively large major population indicate this tephra is highly likely to be the Tsoyowata ash and the intermediate population being from the same origin further supports this interpretation. It is possible that the intermediate population originated from the surrounding volcanic rock during the eruption that produced the Tsoyowata ash. Given the common and widespread occurrence of tephras from the nearby Mono Craters and that a different tephra interval directly overlies the sampled tephra (LL16-T-02), it is unsurprising that there is a third minor population of Mono Craters tephra. This minor population was probably derived from depositional reworking or sampling error (i.e. sampling too close to the perimeter that may have been disturbed during coring or extrusion).

4.4.2 Age-Depth Modeling

Radiocarbon, tephrochronology, and ^{210}Pb dates were all input to *Bacon* (Blaauw and Christen, 2011) for both Lyell and Maclure cores to produce age-depth models with a probability distribution and 95% confidence envelope. In the Lyell core age-depth model, the mean 95% confidence range is 1054 years, the best constrained 95% confidence range is 11.3 years at 1 cm, and the least constrained 95% confidence range is 1781.1 years at 93 cm (Figure 21). Lyell core sedimentation rates average ~0.2 mm/yr with a marked increase to ~0.4 mm/yr from 22-45 cm (~1300-2000 cal yr BP). Sedimentation rates also increased above average to ~0.27 mm/yr in the uppermost 6 cm, or last ~200 years. In the Maclure core

age-depth model, the mean 95% confidence range is 673 yr, the best constrained 95% confidence range is 125 yr at 1 cm, and the least constrained 95% confidence range is 1205 yr at 80 cm (Figure 22). Maclure core sedimentation rates are ~0.10 mm/yr before 3200 cal yr BP, rising to peak rates near 0.30 mm/yr between ~1700-3200 cal yr BP, then lowering again to ~0.17 mm/yr after 1700 cal yr BP.

4.5 CRN Exposure Dating Analysis

I assessed the CRN exposure ages from the LLNL study using the reduced chi-squared statistic to evaluate different moraines, ridges and groupings of CRN ages from the LLNL study for geologic scatter versus measurement uncertainty. Twenty-one exposure ages from the Lyell moraines vary from ~0.1-1.2 ka but the majority cluster around ~0.3 ka (Figure 8). There does not appear to be a significant difference in ages between inner and outer ridges of the Lyell moraines. When lumped together, the ages from these moraines results in a χ_R^2 equal to ~30. If the five exposure ages older or younger than the late-LIA (<150 and >350 yr) are considered outliers and removed, the resulting chi-squared value is ~1.4. Upon removal of anomalous ages, individual Lyell moraines/ridges all display mean ages ranging from 263-289 yr and have χ_R^2 1.35 or under, with the exception of LyelWB where $\chi_R^2 = \sim 4$.

Ten exposure ages from the Maclure moraines vary from ~0.6-4.5 ka. Most CRN ages from the inner two moraine ridges are younger (~0.6-1.6 ka) than those from the outer two moraine ridges (~2.2-4.5 ka). The χ_R^2 values cannot be calculated for MACC and MACBY because each has only one CRN age. The CRN ages from MACA produce a χ_R^2 equal to ~100 and the CRN ages from MACB give a χ_R^2 of ~19. When the ages are considered by each individual cluster shown in the summary curve (see "Sum" data in Figure 9), however, all χ_R^2 values are below one. These clustered ages are centered on 3.0, 2.3, and 1.0 ka.

Thirteen exposure ages from the Mt Price moraines vary from 2.5-10.8 ka. Three ages from PRCW1 have yet to be analyzed. The χ_R^2 equals ~2 for moraine PRCE with an average age of ~8.1 ka. The χ_R^2 equals ~19 for moraine PRCC with an average age of ~4.2 ka. Based off the two existing CRN

ages, χ_R^2 equals ~0.3 for moraine PRCW1 with an average age of ~10.5 ka. If the oldest age is removed from the PRCE data set, the χ_R^2 is ~0.5. When the two clusters of ages for moraine PRCC are analyzed individually, the oldest cluster (~5.6 ka) has a χ_R^2 of ~0.2 and the youngest cluster (~2.7 ka) has a χ_R^2 of ~0.5.

5.0 Discussion

5.1 Glaciolacustrine record of Neoglaciation

5.1.1 Lyell Glacier

Rock flour is commonly characterized by high MS values, low LOI, and increased fine sediments, generally fine silt but can range from clay to coarse silt (Karlén, 1976; Dahl et al., 2003). These key attributes are exemplified by the most prominent clastic interval (42-20 cm depth) and, to a lesser degree, from ~13-4 cm depth of the Lower Lyell Lake core. The peak in fine silt during the prominent clastic interval from 42-20 cm depth, where MS is high and LOI is low, indicates fine silt is likely the best proxy for rock flour in the Lower Lyell Lake core. Of note is that fine silt percentage is consistently high during the highly organic intervals lower in the core. These older fine silt intervals likely represent aeolian sediment (indicated by low MS, high LOI), or may also be due, in part, to diatoms that persisted through lab pretreatment. Interestingly, fine sand percentages increase in the top 42 cm compared to the bottom of the core. Although during the most pronounced intervals of rock flour fine sand percentage drops, overall it does seem to increase during intervals of interpreted glacier presence in the cirque.

Apparent onset of Neoglaciation in the west Lyell cirque is recorded by rock flour deposition in Lower Lyell Lake beginning at ~1830 cal yr BP. This rock flour interval peaks around ~1790 cal yr BP then steadily decreases until it largely disappears ~1230 cal yr BP. This fading rock flour sequence likely indicates glacier recession because smaller glaciers (smaller extent and volume) cause less abrasion and,

thus, produces less rock flour that is subsequently deposited downstream. A subsequent glacial interval lasts from ~610-80 cal yr BP with the glacial maxima centered around ~460 cal yr BP. This sequence broadly agrees with glacial intervals documented at the Palisade and Conness glaciers by Bowerman and Clark (2011) and Konrad and Clark (1998), respectively, although it does represent a later onset of Neoglaciation by nearly 1500 years than at either of those two sites. The record at lower Lyell Lake does not preclude earlier advances, however, but rather may represent differing sensitivities of rock flour deposition in the various sites. The smaller lakes upstream of Lower Lyell Lake capture some of the rock flour flux from the west Lyell Glacier lobe, possibly preventing rock flour from smaller, earlier advances from reaching Lower Lyell Lake.

Although the timing of glacial maxima in the Lyell core is generally consistent with other glaciolacustrine records in the region, the timing with respect to apparent magnitude is at odds with those records which indicate the largest glacial advances occurred during late-LIA. Historical records also support a late-LIA Holocene glacial maximum, as indicated by the ice extent in Russell's map and photos (Figure 5; Russell, 1889). This discrepancy between the glaciolacustrine records and historical records may be explained by the boundaries of the local drainage basins of the respective western lobe and eastern lobe of the Lyell Glacier. The western lobe moraine, which I targeted in this study, straddles a drainage divide between outwash feeding Lower Lyell Lake and the drainage to the east. This divide indicates that a significant amount of the rock flour produced during the most extensive glacier advance was transported farther down Lyell Canyon, effectively bypassing Lower Lyell Lake. Conversely, smaller glacial advances (e.g., to the current extent) may have drained entirely into Lower Lyell Lake (Figure 11). If this were the case, smaller early glacial advances would deposit larger proportions of rock flour in the cored lake compared to subsequent larger glacial advances. An alternative hypothesis to explain the late Neoglacial onset in the Lyell core is that meltwater from earlier glacial advances drained entirely into the eastern drainage. This idea is not supported by current topography, however, and although glaciers do commonly erode and thus change subglacial topography, the bedrock acting as the drainage divide would be in the ablation zone regardless of the glacier size, where the glacier is depositing rather than eroding.

This makes it unlikely that these Neoglacial advances significantly eroded the bedrock topography to alter the drainage divide. For these reasons, I favor the former hypothesis to explain the discrepancy between the Lyell glaciolacustrine record and prior records. Both ideas could be tested by coring two of the lakes farther downstream that capture outwash from the eastern portions of the Lyell Glacier. These lakes were not cored for this study, however, because they are shallow and, thus, more susceptible to drying out and sedimentological changes related to fluvial processes (e.g., channel migration, sub-glacial stream flow, delta progradation) that would tend to obscure a purely glaciologic rock flour record.

5.1.2 Maclure Glacier

As with the Lower Lyell Lake record, I interpret rock flour intervals in the Maclure Lake record based on the characteristic high MS values, fine-grained intervals (relative increases in clay, fine silt, and coarse silt), and low LOI values. However, the rock flour signal is less clear in the core from Maclure Lake (LM16-01-01). Coarse sandy intervals, prevalent throughout much of the core, have extremely low LOI percentages. So, although rock flour intervals exhibit low absolute LOI values, they sometimes represent an increase from the surrounding stratigraphy. Visual stratigraphy and relative amounts of diatoms were also considered when interpreting the rock flour signal. Rock flour is usually grey-blue in color versus tones of brown for non-glacial (e.g., aeolian) fine grained sediments (Dahl et al., 2003) and should not contain large proportions of diatoms, which would represent increased biologic productivity rather than increased clastic deposition.

Apparent onset of Neoglaciation in the Maclure cirque is recorded by initial rock flour deposition at ~1650 cal yr BP. This early rock flour interval persisted until ~1280 cal yr BP. A more substantial interval of rock flour deposition occurs from ~1020-370 cal yr BP with the apparent Holocene rock flour maximum at ~970 cal yr BP. The timing of these glacial advances generally aligns with glacial intervals recorded by Bowerman and Clark (2011) and Konrad and Clark (1998), although as for the Lower Lyell Lake record, it represents an onset of Neoglaciation that is later than those earlier studies by ~1650 years.

As with the Lower Lyell Lake record, this difference may not mean those earlier advances did not occur at Maclure cirque; two lakes above Maclure lake may have trapped most or all the rock flour related to such earlier events. Furthermore, the glacial intervals recorded in Maclure Lake do not directly parallel those in Lower Lyell Lake, with the Maclure Glacier apparently advancing later and retreating earlier.

This asynchrony in the glaciolacustrine records from Maclure Lake and Lower Lyell Lake may be due to several factors. As mentioned above, each of the paternoster lakes in this cirque has a different sensitivity of rock flour deposition. Lakes farther upstream, closer to the glacier, usually provide more sensitive records of smaller glacial fluctuations while lakes farther downstream (e.g., Maclure Lake) are likely more sensitive to larger scale glacial fluctuations (Dahl et al., 2003). These differing sensitivities could result in slight offsets to the timing of rock flour deposition. Compounding this is the larger potential for gruss deposition in the Maclure Lake that may obscure rock flour deposition. Another possible explanation for the difference is that the Lyell and Maclure glaciers have different glacial dynamics. For instance, currently the Maclure glacier is still flowing while the larger Lyell Glacier has stagnated. This, in large part, reflects the larger and steeper cirque headwall that provides the Maclure Glacier orographic shielding and, thus, cooling (Graf, 1976; Clark et al., 1994). Additionally, rockfall events and increased surficial debris flux can reduce ablation rates and alter how larger scale climatic forcings affect each glacier (Clark et al., 1994). Lastly, the age models may not be accurate for smaller scale sedimentation rates that are probably more variable than the model indicates. Coarse sandy sediments, present in both the Lyell and Maclure cores, should represent briefer, higher energy deposition than finer-grained intervals. Thus, these coarse-grained intervals may represent shorter periods than the age model indicates and vice versa for finer-grained intervals.

The fine-grained intervals near the bottom of the core from 94-80 cm (~5920-4590 cal yr BP) and 77-62 cm (~4290-3020 cal yr BP) were not interpreted as rock flour for several reasons. Although LOI values are still relatively low, they are consistently higher than the fine-grained intervals in the upper third of the core. This observation is supported by smear slide analysis, which showed much higher proportions of diatoms versus clastic grains in the lower intervals compared to the rock flour intervals higher up in the

core. Low LOI values in the earlier fine-grained intervals are also influenced locally by thin sandy layers nestled in between, which have very low LOI values. The resolution of sampling could not isolate solely fine-grained from coarse-grained intervals, so higher LOI values such as those at 70.5 cm and 91 cm depth may be more representative of these fine sediments (Figure 17). It is interesting to note that, although these intervals do not appear to be glacial in origin, they do overlap with the later portion of the Garibaldi Phase that lasted from ~7350-5770 cal yr BP as well as several other glacial advances in the North Cascades mountain range and western Canada (Menounos et al., 2009; Ryder and Thomson, 1986). Although no Neoglacial advances have been recognized earlier than ~3400 cal yr BP in the Sierra Nevada, Bowerman and Clark (2011) also noted a minor increase of fine-grained, higher MS/lower organic clastic sediments in First and Second lakes below the Palisade Glacier between ~5400-4800 cal yr BP. If these intervals from both the Maclure and Palisade glaciolacustrine records are indeed glacial rock flour, it would indicate a much earlier onset of Neoglaciation in the Sierra Nevada than currently documented.

Coarse sandy intervals in the Maclure Lake cores are most likely weathered gruss sourced from the surrounding bedrock-dominated slopes, rather than from glacial meltwater. Outwash from the glacier must pass through two lakes before entering Maclure Lake, and then cross the deepest portion of Maclure Lake before deposition at the shallower bench I cored near the outlet of the lake. It is highly unlikely that such coarse sediments could remain in suspension through that sequence. A non-glacial origin to the sediments is further supported by very low associated MS values, indicating greater weathering than is typical for glacial rock flour. Gruss is abundant in joint fractures and small flats on the bedrock adjoining the lake. These sediments are unlikely to be mobilized and transported to the lake by gradual snowmelt or under a snowpack; instead, I conclude these intervals of enhanced gruss deposition to the lake likely represent mobilization during periods of more intense summer rainstorms.

5.1.3 Mt Price glaciers

The majority of the Lake Aloha core record comprises high organic gyttja with no evidence of significant glacial rock flour in the proxies or visual stratigraphy. The only peak in MS from LA16-G02 is coincident with the thick basal tephra deposit, assumed to be the Tsoyowata ash based on other records in the area (e.g., Clark and Gillespie, 1997; Noble et al., 2016). The tephra deposit contains little to no clastic grains but does contain diatoms, likely related in part to liquefaction and mixing with higher organic gyttja during transport. It is possible that the boulder-rich ridges previously mapped as Neoglacial moraines are actually remnants of paraglacial processes such as pronival (protalus) ramparts. This alternative origin for these landforms would explain why there is no significant rock flour preserved in the Lake Aloha core. Clark and Gillespie (1997) also cored a small tarn upslope of Lake Aloha within the Price drainage and found no evidence of glacier advances post-Recess Peak. Pronival ramparts are distinct ridges of rock debris, usually angular and boulder dominated, formed at the lower margin of a perennial snowbed / firn field. The snowbed facilitates sliding of rockfall debris from the respective headwall to the toe of the snowbed where the rocky debris is accumulated (Shakesby, 1997; Hedding, 2011; Hedding and Sumner, 2013). These features often resemble glacial moraines and have been misinterpreted as such in previous studies (Brook and Williams, 2013). This landform interpretation is inconsistent, however, with the extremely clean, stripped nature of the bedrock between the steep cirque headwalls and the presumed moraines as well as the overall size of the landforms in question when compared to defined pronival rampart criteria which are generally smaller in extent (Hedding and Sumner, 2013). Thus, I suggest that these landforms may indeed be true moraines, albeit formed from small “glacierettes” with minor flow and subglacial abrasion. It is unsurprising that these small glaciers may not have produced enough rock flour to be detected in the lake sediment record.

5.2 ^{10}Be CRN dating

CRN dating of these glacial deposits presents an exceptional data set for Holocene moraines in the Sierra Nevada, but they also indicate a complex geomorphic record. Taken at face value, they suggest a very complex glacial history. Conversely, they may suggest that such small, young moraines incorporate non-glacial processes that complicate the exposure histories. In this section, the CRN ages are assessed at each field site with respect to each respective glaciolacustrine record as well as prior research and historical records.

5.2.1 Lyell Glacier

Overall the Lyell ^{10}Be CRN ages match well with both historical records and the glaciolacustrine record (Figure 23). All Lyell CRN ages are young, most falling within the late-LIA. The ages clustered in the late-LIA have a χ_R^2 close to 1, which indicates very little geologic scatter. The timing of this glacial advance is consistent with prior research in the area (e.g., Russell, 1889; Konrad and Clark, 1998; Bowerman and Clark, 2011). The only inconsistency is the magnitude of glacial advances as indicated by the Lyell rock flour record. The watershed divide for the western lobe of the Lyell Glacier at peak glacial extent may explain this apparent discrepancy (see section *5.1.1*). This would result in a diminished rock flour record during peak Neoglacial extent because it indicates that outwash from the eastern portion of the glacier would effectively bypass Lower Lyell Lake. Overall though, ^{10}Be CRN dating below the Lyell Glacier appears to provide viable age constraints for boulder emplacement along these moraines.

5.2.2 Maclure Glacier

CRN ages for the Maclure Glacier span a much greater range than those of the adjoining Lyell Glacier. It is particularly noteworthy that there is a complete absence of late-LIA ages present, directly conflicting with historical mapping and observations (Russell, 1889) as well as the extremely youthful appearance of the moraines (e.g., angular, unweathered clasts, absence of vegetation or lichen, steep, unstable slopes). Furthermore, the two older age clusters predate the earliest rock flour intervals

documented in the Maclure Lake sedimentary record. However, there is also a notable lack of early Holocene exposure ages such as those of the Price cirque moraines. If the Maclure CRN ages are older than late-LIA strictly because of inheritance from prior exposure, I would expect them to have a more stochastic distribution spanning the entire Holocene. Instead, all but one age (4.5 ka) fall within the Neoglacial period documented by Bowerman and Clark (2011) and Konrad and Clark (1998), and the ages appear to fall into several clusters rather than being completely random. For these reasons, I suspect the CRN age distribution at Maclure Glacier is not simply a function of inheritance due to boulder positioning and/or inadequate erosion, but also not necessarily a direct record of glacier advance and deposition as moraine records are traditionally regarded. Recent studies on CRN dating of debris-covered glaciers and ice-cored moraines may yield insight into this predicament.

Although not directly observed, I infer that the Maclure moraines are likely ice-cored moraines. They comprise numerous steep, morphologically fresh lobate ridges and furrows, with abundant unstable boulders and the steep cirque headwall provides a ready source of coarse supraglacial debris. These are common characteristics of debris-covered glaciers, which are abundant in the Sierra Nevada (Clark et al., 1994). In such ice-cored moraines, continuous supraglacial debris of only a few centimeters can dramatically reduce ablation rates in the ice core, particularly in cold, high alpine sites (Östrem, 1959; Clark et al., 1994; Nicholson and Benn, 2006). As a result, the ice core can persist well after the adjoining clean-ice portion of a glacier has thinned and retreated, effectively stranding the debris-covered toe of the glacier (Clark et al., 1994; Rowan et al., 2015; Anderson and Anderson, 2016; Crump et al., 2017).

Crump et al. (2017) used CRN exposure dating for Neoglacial ice-cored moraines from Baffin Island, Artic Canada. They suggest that the oldest ages, after removing samples with presumed inheritance, are indicative of initial moraine formation. Using the numerical model developed by Anderson and Anderson (2016), Crump et al. (2017) showed that glaciers can reconnect with an ice-cored moraine after prior retreat, effectively reactivating the ice core as part of the glacier rather than obliterating it. As a result, ice-cored moraines can represent several different advances, amalgamated together through the various retreats and subsequent advances. Through these retreats and advances, some

boulders may maintain their original positions and record constant exposure from initial moraine formation while others may slide, rotate, fall, or become buried, resulting in younger ages. Although Crump et al. (2017) did not observe any obvious zoning of exposure ages in their study, results from the Maclure moraines suggest a general fit to this model, with younger ages dominating on inner moraines and older ages on outer moraines: ages on the two outermost moraines are all greater than 2.2 ka and cluster between 2.2 and 3.2 ka (broadly consistent with onset of Neoglaciation in the range as determined in previous studies) and all but one age on the inner two moraines are 1.6 ka or younger. Given that it is likely that at least some of these boulders have some prior exposure (thus providing a possible explanation for the oldest ages on each moraine set), the clustered ages may record early (pre-LIA) advances of the Maclure Glacier not recorded in the adjacent, cleaner Lyell Glacier. Because of the small sample size, however, this interpretation remains speculative.

Fieldwork to provide direct evidence of an ice core in the Maclure moraines would validate my interpretations of the geomorphic processes influencing the exposure history of boulders along the moraines. To do this, I would need to search the Maclure moraines for ice exposures created from melt-out and erosion, which would reveal the inner contents of the moraine. Other work to provide clarity to these CRN ages could include more sophisticated inheritance versus moraine degradation models to determine true age (e.g., Applegate et al., 2010, 2012) and/or determine if geologic scatter or measurement uncertainty is responsible for variations in exposure ages using the independent ^{10}Be and ^{26}Al CRN ages (e.g., Balco, 2011).

5.2.3 Mt Price glaciers

Although the different moraines and clusters within the Price moraine CRN ages appear to have robust reduced chi-squared values, given the regional context, it seems unlikely that ^{10}Be CRN ages accurately record glacial events in this area. The Lake Aloha sediment cores (LA16-G01 & LA16-G02) do not record any late-Holocene rock flour intervals, and no other glacier advances have been recorded in

the Sierra Nevada (or most other ranges in the American Cordillera) during the majority of the CRN age intervals (~5.5-11 ka). It is possible that the youngest grouping (~2.7 ka) does have a glacial influence because it does overlap with documented glacial advances in the range (Figure 23). It is apparent, however, that other non-glacial geomorphic processes influence the CRN exposure ages at this site.

The most obvious process, inheritance, could influence these boulders through several means. Prior exposure on valley walls and subglacial bedrock before glacial transport is a commonly acknowledged problem (Putkonen and Swanson, 2003; Ivy-Ochs et al., 2007). In this case, if the side of the boulder that experienced prior exposure is sampled, it will contain multiple exposure histories and appear older than the true age of the landform (Balco, 2011). Another complication could result from reworking boulders from older moraines rather than obliterating them completely (Ivy-Ochs et al., 2007; Balco, 2011; Li et al., 2016). In this process, exposure histories from prior moraines can persist through subsequent advances. In particular, smaller glaciers, such as those in the Price cirque, may lack the erosive power to strip prior CRN accumulations on rocky debris from headwalls and plucked bedrock. Li et al. (2016) also proposed this for their study using ^{10}Be CRN exposure dating on boulders emplaced in presumed LIA moraines in the eastern Tian Shan mountain range in China. Like the Lyell, Maclure, and Price glaciers, larger and thicker glaciers in the Tian Shan produced young, well clustered exposure ages within the LIA. Conversely, small and thin glaciers produced widely scattered exposure ages, up to tens of thousands of years older than expected. The small glacier sizes that produced inheritance prone CRN data ($\leq$0.4 km^2) in the Tian Shan is consistent with the Lyell, Maclure, and Price glaciers, with a maximum extent of 0.037 km^2 in the Price cirque (Table 3).

It seems likely that the widely contrasting Price CRN ages likely reflect all the inheritance issues listed above. The extremely steep cirque headwalls in the Price cirque would supply a surplus of boulder debris prone to inheritance. Episodic rockfall events (possibly triggered by earthquakes) as the dominant source of debris could explain the clustering of ages. A lack of glacial polish and/or striations on the sampled boulders strengthen the argument for a headwall origin versus plucked bedrock for these moraines. Likewise, glaciers of this size should not be expected to abrade these boulders to sufficiently

remove all prior CRN accumulation and the lack of evidence for boulder abrasion furthers this argument. The complete absence, however, of any young CRN ages, despite the youthful appearance of these moraines, remains difficult to explain. Reworking prior deposits and or rockfall debris, without significant erosion of said deposits, may offer an explanation. If the sampled boulders have undergone several disturbances that resulted in reorientation, then each exposed side would exhibit a different exposure history, all older than the most recent emplacement along the modern moraines. These results suggest that smaller glaciers, particularly those near the transition zone from ice field to glacier, are not well suited for CRN exposure dating, at least not in the Sierra Nevada mountain range.

6.0 Conclusions

I collected glaciolacustrine cores in the Sierra Nevada from below three different moraine complexes with widely varied CRN ages that are markedly older than historical records and research in the area suggest for moraine formation. I used these two independent records of glacial fluctuations to determine if CRN dating was accurately recording glacier fluctuations or if other geomorphic processes were influencing CRN ages for each site. Apparent onset of Neoglaciation for the Lyell Glacier, indicated by rock flour deposition in the glaciolacustrine record, begins at ~1830 cal yr BP and lasts through ~1230 cal yr BP with peak rock flour deposition at ~1790 cal yr BP. Another advance occurred from ~610-80 cal yr BP peaking at ~460 cal yr BP. In the Maclure lacustrine record, glacial fluctuations occurred from ~1650-1280 cal yr BP and ~1020-370 cal yr BP with the apparent Holocene maximum ~970 cal yr BP. No rock flour record is apparent from the Lake Aloha sediment core, from below the Price cirque.

The well clustered late-LIA CRN ages for the Lyell moraines match well with the published record of Neoglacial activity in the Holocene. Discrepancies between these ages and the constraints from the glaciolacustrine record collected at Lower Lyell Lake appear to largely reflect limitations with the lake core record rather than problems related to CRN dating. The contrasting CRN moraine ages from the

adjoining Maclure Glacier, including absence of late-LIA ages and clusters of older ages at ~3.0, 2.3, and 1.0 ka, may reflect the influence of glacier dynamics of ice-cored moraines. This hypothesis is consistent with the Maclure moraine morphology and would account for the apparent clustering of CRN ages within the Neoglacial period defined by prior studies (~3200 cal yr BP to late-LIA; Konrad and Clark, 1998; Bowerman and Clark, 2011). Ice cored moraines can be reincorporated into subsequent glacial advances rather than obliterated and present several moraines incorporated together, effectively yielding CRN ages from multiple Neoglacial events. If the older clusters of Maclure CRN ages do in fact record Neoglacial advances, the apparent lack of concomitant rock flour deposition in Maclure Lake would suggest the advances were too small to cause measurable rock flour deposition in the lake. Thus, the timing and extent of the Maclure record is broadly consistent with other records, with the last glacial advance being the largest. In contrast to the records from Lyell and Maclure glaciers, the wide range of CRN ages from the Price moraines seem to indicate systematic problems with inheritance rather than true glacial events. These older ages are probably caused by a combination of prior exposure on the headwall before glacier transport, reworking prior deposits that accumulated additional CRNs, and insufficient abrasion to strip boulders of these prior CRN concentrations before emplacement on the current moraine. Based on these glacial systems, I suggest the use of CRN exposure dating on moraines from such small glaciers are highly susceptible to inheritance whereas larger glaciers (e.g., Lyell Glacier) seem to produce cleaner records that more accurately record moraine formation. Additionally, ice-cored moraines yield complex CRN chronologies that may not be well-suited for use in applications of climatic significance.

7.0 References

Anderson, L.S., and Anderson, R.S., 2016, Modeling debris-covered glaciers: response to steady debris deposition: The Cryosphere, v. 10, p. 1105–1124, doi: 10.5194/tc-10-1105-2016.

Appleby, P.G., and Oldfield, F., 1978, The calculation of lead-210 dates assuming a constant rate of supply of unsupported 210Pb to the sediment: CATENA, v. 5, p. 1–8, doi: 10.1016/S0341-8162(78)80002-2.

Applegate, P.J., Urban, N.M., Keller, K., Lowell, T.V., Laabs, B.J.C., Kelly, M.A., and Alley, R.B., 2012, Improved moraine age interpretations through explicit matching of geomorphic process models to cosmogenic nuclide measurements from single landforms: Quaternary Research, v. 77, p. 293–304, doi: 10.1016/j.yqres.2011.12.002.

Applegate, P.J., Urban, N.M., Laabs, B.J.C., Keller, K., and Alley, R.B., 2010, Modeling the statistical distributions of cosmogenic exposure dates from moraines: Geoscientific Model Development, v. 3, p. 293.

Bacon, C.R., 1983, Eruptive history of Mount Mazama and Crater Lake Caldera, Cascade Range, U.S.A.: Journal of Volcanology and Geothermal Research, v. 18, p. 57–115, doi: 10.1016/0377-0273(83)90004-5.

Bakke, J., Nesje, A., Dahl, S.O., and others, 2005, Utilizing physical sediment variability in glacier-fed lakes for continuous glacier reconstructions during the Holocene, northern Folgefonna, western Norway: The Holocene, v. 15, p. 161–176.

Balco, G., 2011, Contributions and unrealized potential contributions of cosmogenic-nuclide exposure dating to glacier chronology, 1990–2010: Quaternary Science Reviews, v. 30, p. 3–27, doi: 10.1016/j.quascirev.2010.11.003.

Barclay, D.J., Wiles, G.C., and Calkin, P.E., 2009, Holocene glacier fluctuations in Alaska: Quaternary Science Reviews, v. 28, p. 2034–2048, doi: 10.1016/j.quascirev.2009.01.016.

Basagic, H.J., 2008, Quantifying Twentieth Century Glacier Change in the Sierra Nevada, California: Portland State University, 115 p.

Basagic, H.J., and Fountain, A.G., 2011, Quantifying 20th Century Glacier Change in the Sierra Nevada, California: Arctic, Antarctic, and Alpine Research, v. 43, p. 317–330, doi: 10.1657/1938-4246-43.3.317.

Bertrand, S., Araneda, A., Vargas, P., Jana, P., Fagel, N., and Urrutia, R., 2012, Using the N/C ratio to correct bulk radiocarbon ages from lake sediments: Insights from Chilean Patagonia: Quaternary Geochronology, v. 12, p. 23–29, doi: 10.1016/j.quageo.2012.06.003.

Blaauw, M., and Christen, A., 2011, Flexible Paleoclimate Age-Depth Models Using an Autoregressive Gamma Process: Bayesian Analysis, v. 6, p. 457–474, doi: 10.1214/11-BA618.

Bowerman, N.D., and Clark, D.H., 2011, Holocene glaciation of the central Sierra Nevada, California: Quaternary Science Reviews, v. 30, p. 1067–1085, doi: 10.1016/j.quascirev.2010.10.014.

Briner, J.P., Kaufman, D.S., Manley, W.F., Finkel, R.C., and Caffee, M.W., 2005, Cosmogenic exposure dating of late Pleistocene moraine stabilization in Alaska: Geological Society of America Bulletin, v. 117, p. 1108–1120.

Brook, M.S., and Williams, J., 2013, A Relict Pronival (Protalus) Rampart in the Tararua Range, North Island, New Zealand: Pronival (Protalus) Rampart in New Zealand: Permafrost and Periglacial Processes, v. 24, p. 67–74, doi: 10.1002/ppp.1759.

Brugger, K.A., 2007, Cosmogenic 10Be and 36Cl ages from Late Pleistocene terminal moraine complexes in the Taylor River drainage basin, central Colorado, USA: Quaternary Science Reviews, v. 26, p. 494–499, doi: 10.1016/j.quascirev.2006.09.006.

Calkin, P.E., Wiles, G.C., and Barclay, D.J., 2001, Holocene coastal glaciation of Alaska: Quaternary Science Reviews, v. 20, p. 449–461.

Clark, D.H., 1995, Extent, timing, and climatic significance of latest Pleistocene and Holocene glaciation in the Sierra Nevada [Ph.D. dissertation]: University of Washington, 193 p.

Clark, D.H., Clark, M.M., and Gillespie, A.R., 1994, Debris-Covered Glaciers in the Sierra Nevada, California, and Their Implications for Snowline Reconstructions: Quaternary Research, v. 41, p. 139–153, doi: 10.1006/qres.1994.1016.

Clark, D.H., and Gillespie, A.R., 1997, Timing and significance of Late-glacial and Holocene cirque glaciation in the Sierra Nevada, California: Quaternary International, v. 38–39, p. 21–38, doi: 10.1016/S1040-6182(96)00024-9.

Clark, D.H., Hidy, A.J., Zimmerman, S.H., Finkel, R.C., Stock, G.M., and Schaefer, J.M., 2015, Wide span of exposure ages on Holocene moraines in the Sierra Nevada: process or climatic controls?, https://gsa.confex.com/gsa/2015AM/webprogram/Paper269088.html (accessed November 2015).

Cockburn, H.A.P., and Summerfield, M.A., 2004, Geomorphological applications of cosmogenic isotope analysis: Progress in Physical Geography, v. 28, p. 1–42, doi: 10.1191/0309133304pp395oa.

Crump, S.E., Anderson, L.S., Miller, G.H., and Anderson, R.S., 2017, Interpreting exposure ages from ice-cored moraines: a Neoglacial case study on Baffin Island, Arctic Canada: INTERPRETING EXPOSURE AGES FROM ICE-CORED MORAINES: Journal of Quaternary Science, v. 32, p. 1049–1062, doi: 10.1002/jqs.2979.

Dahl, S.O., Bakke, J., and Nesje, A., 2003, Reconstruction of former glacier equilibrium-line altitudes based on proglacial sites: an evaluation of approaches and selection of sites: Quaternary Science Reviews, v. 22, p. 275–287.

Davis, P.T., Menounos, B., and Osborn, G., 2009, Holocene and latest Pleistocene alpine glacier fluctuations: a global perspective: Quaternary Science Reviews, v. 28, p. 2021–2033, doi: 10.1016/j.quascirev.2009.05.020.

Doughty, A.M., Schaefer, J.M., Putnam, A.E., Denton, G.H., Kaplan, M.R., Barrell, D.J.A., Andersen, B.G., Kelley, S.E., Finkel, R.C., and Schwartz, R., 2015, Mismatch of glacier extent and summer insolation in Southern Hemisphere mid-latitudes: Geology, v. 43, p. 407–410, doi: 10.1130/G36477.1.

Fountain, A.G., and Tangborn, W.V., 1985, The Effect of Glaciers on Streamflow Variations: Water Resources Research, v. 21, p. 579–586, doi: 10.1029/WR021i004p00579.

Glew, J.R., 1991, Miniature gravity corer for recovering short sediment cores: Journal of Paleolimnology, v. 5, p. 285–287.

Gosse, J.C., and Phillips, F.M., 2001, Terrestrial in situ cosmogenic nuclides: theory and application: Quaternary Science Reviews, v. 20, p. 1475–1560.

Graf, W.L., 1976, Cirques as glacier locations: Arctic and Alpine Research, p. 79–90.

Grimm, E.C., Maher, L.J., and Nelson, D.M., 2009, The magnitude of error in conventional bulk-sediment radiocarbon dates from central North America: Quaternary Research, v. 72, p. 301–308, doi: 10.1016/j.yqres.2009.05.006.

Guido, Z.S., Ward, D.J., and Anderson, R.S., 2007, Pacing the post-last glacial maximum demise of the Animas Valley Glacier and the San Juan Mountain ice cap, Colorado: Geology [Boulder], v. 35, p. 739–742, doi: 10.1130/G23596A.1.

Hallet, B., and Putkonen, J., 1994, Surface dating of dynamic landforms: Young boulders on aging moraines: Science, v. 265, p. 937–940.

Hedding, D.W., 2011, Pronival rampart and protalus rampart: a review of terminology: Journal of Glaciology, v. 57, p. 1179–1180, doi: 10.3189/002214311798843241.

Hedding, D.W., and Sumner, P.D., 2013, Diagnostic Criteria for Pronival Ramparts: Site, Morphological and Sedimentological Characteristics: Diagnostic Criteria for Pronival Ramparts: Geografiska Annaler: Series A, Physical Geography, v. 95, p. 315–322, doi: 10.1111/geoa.12021.

Huber, N.K., Bateman, P.C., Wahrhaftig, C., Aitken, D., and Phillips, E., 2003, Geologic Map of Yosemite National Park and Vicinity, California: a digital database: U.S. Geological Survey, http://pubs.usgs.gov/imap/i1874/ (accessed April 2016).

Ivy-Ochs, S., Kerschner, H., and Schlüchter, C., 2007, Cosmogenic nuclides and the dating of Lateglacial and Early Holocene glacier variations: The Alpine perspective: Quaternary International, v. 164–165, p. 53–63, doi: 10.1016/j.quaint.2006.12.008.

Karlén, W., 1981, Lacustrine Sediment Studies. A Technique to Obtain a Continous Record of Holocene Glacier Variations: Geografiska Annaler. Series A, Physical Geography, v. 63, p. 273, doi: 10.2307/520840.

Karlén, W., 1976, Lacustrine Sediments and Tree-Limit Variations as Indicators of Holocene Climatic Fluctuations in Lappland, Northern Sweden: Geografiska Annaler: Series A, Physical Geography, v. 58, p. 1–34, doi: 10.1080/04353676.1976.11879921.

Kirkbride, M.P., and Winkler, S., 2012, Correlation of Late Quaternary moraines: impact of climate variability, glacier response, and chronological resolution: Quaternary Science Reviews, v. 46, p. 1–29, doi: 10.1016/j.quascirev.2012.04.002.

Konrad, S.K., and Clark, D.H., 1998, Evidence for an Early Neoglacial Glacier Advance from Rock Glaciers and Lake Sediments in the Sierra Nevada, California, U.S.A.: Arctic and Alpine Research, v. 30, p. 272, doi: 10.2307/1551975.

Larsen, C.P.S., Pienitz, R., Smol, J.P., Moser, K.A., Cumming, B.F., Blais, J.M., MacDonald, G.M., and Hall, R.I., 1998, Relations between lake morphometry and the presence of laminated lake sediments: a re-examination of Larsen and MacDonald (1993): Quaternary Science Reviews, v. 17, p. 711–717.

Leonard, E.M., 1989, Climatic Change in the Colorado Rocky Mountains: Estimates Based on Modern Climate at Late Pleistocene Equilibrium Lines: Arctic and Alpine Research, v. 21, p. 245, doi: 10.2307/1551563.

Leonard, E.M., 1985, Glaciological and climatic controls on lake sedimentation, Canadian Rock Mountains: Zeitschrift fur gletscherkunde und glazialgeologie, v. 21, p. 35–42.

Leonard, E.M., 1986, Varve studies at Hector Lake, Alberta, Canada, and the relationship between glacial activity and sedimentation: Quaternary Research, v. 25, p. 199–214, doi: 10.1016/0033-5894(86)90057-8.

Li, Y., Li, Y., Harbor, J., Liu, G., Yi, C., and Caffee, M.W., 2016, Cosmogenic 10Be constraints on Little Ice Age glacial advances in the eastern Tian Shan, China: Quaternary Science Reviews, v. 138, p. 105–118, doi: 10.1016/j.quascirev.2016.02.023.

Licciardi, J.M., Clark, P.U., Brook, E.J., Elmore, D., and Sharma, P., 2004, Variable responses of western US glaciers during the last deglaciation: Geology, v. 32, p. 81–84.

Marcott, S.A., Shakun, J.D., Clark, P.U., and Mix, A.C., 2013, A Reconstruction of Regional and Global Temperature for the Past 11,300 Years: Science, v. 339, p. 1198–1201, doi: 10.1126/science.1228026.

Margold, M., Stroeven, A.P., Clague, J.J., and Heyman, J., 2014, Timing of terminal Pleistocene deglaciation at high elevations in southern and central British Columbia constrained by 10Be exposure dating: Quaternary Science Reviews, v. 99, p. 193–202, doi: 10.1016/j.quascirev.2014.06.027.

Matthews, J., Dahl, S.O., Nesje, A., Berrisford, M.S., and Carin Andersson, 2000, Holocene glacier variations in central Jotunheimen, southern Norway based on distal glaciolacustrine sediment cores: Quaternary Science Reviews, v. 19, p. 1625–1647, doi: 10.1016/S0277-3791(00)00008-1.

Meier, M.F., 1962, Proposed definitions for glacier mass balance terms: Journal of Glaciology, v. 4, p. 252–261.

Meier, M.F., Dyurgerov, M.B., Rick, U.K., O'Neel, S., Pfeffer, W.T., Anderson, R.S., Anderson, S.P., and Glazovsky, A.F., 2007, Glaciers Dominate Eustatic Sea-Level Rise in the 21st Century: Science, v. 317, p. 1064–1067, doi: 10.1126/science.1143906.

Menounos, B., Osborn, G., Clague, J.J., and Luckman, B.H., 2009, Latest Pleistocene and Holocene glacier fluctuations in western Canada: Quaternary Science Reviews, v. 28, p. 2049–2074, doi: 10.1016/j.quascirev.2008.10.018.

Mood, B.J., and Smith, D.J., 2015, Holocene glacier activity in the British Columbia Coast Mountains, Canada: Quaternary Science Reviews, v. 128, p. 14–36, doi: 10.1016/j.quascirev.2015.09.002.

Moore, R.D., Fleming, S.W., Menounos, B., Wheate, R., Fountain, A., Stahl, K., Holm, K., and Jakob, M., 2009, Glacier change in western North America: influences on hydrology, geomorphic hazards and water quality: Hydrological Processes, v. 23, p. 42–61, doi: 10.1002/hyp.7162.

Muir, J., 1875, Living Glaciers of California: Harper's New Monthly Magazine

Myrbo, A., 2005, Initial Core Description (ICD): Overview:, http://lrc.geo.umn.edu/laccore/assets/pdf/sops/icd.pdf.

Nicholson, L., and Benn, D.I., 2006, Calculating ice melt beneath a debris layer using meteorological data: Journal of Glaciology, v. 52, p. 463–470.

Noble, P.J., Ball, G.I., Zimmerman, S.H., Maloney, J., Smith, S.B., Kent, G., Adams, K.D., Karlin, R.E., and Driscoll, N., 2016, Holocene paleoclimate history of Fallen Leaf Lake, CA., from geochemistry and sedimentology of well-dated sediment cores: Quaternary Science Reviews, v. 131, p. 193–210, doi: 10.1016/j.quascirev.2015.10.037.

Osborn, G., Menounos, B., Ryane, C., Riedel, J., Clague, J.J., Koch, J., Clark, D., Scott, K., and Davis, P.T., 2012, Latest Pleistocene and Holocene glacier fluctuations on Mount Baker, Washington: Quaternary Science Reviews, v. 49, p. 33–51, doi: 10.1016/j.quascirev.2012.06.004.

Östrem, G., 1959, Ice melting under a thin layer of moraine, and the existence of ice cores in moraine ridges: Geografiska Annaler, v. 41, p. 228–230.

Phillips, F.M., Zreda, M., Plummer, M.A., Elmore, D., and Clark, D.H., 2009, Glacial geology and chronology of Bishop Creek and vicinity, eastern Sierra Nevada, California: Geological Society of America Bulletin, v. 121, p. 1013–1033, doi: 10.1130/B26271.1.

Putkonen, J., and Swanson, T., 2003, Accuracy of cosmogenic ages for moraines: Quaternary Research, v. 59, p. 255–261, doi: 10.1016/S0033-5894(03)00006-1.

Putnam, A.E., Schaefer, J.M., Denton, G.H., Barrell, D.J.A., Andersen, B.G., Koffman, T.N.B., Rowan, A.V., Finkel, R.C., Rood, D.H., Schwartz, R., Vandergoes, M.J., Plummer, M.A., Brocklehurst, S.H., Kelley, S.E., et al., 2013, Warming and glacier recession in the Rakaia valley, Southern Alps of New Zealand, during Heinrich Stadial 1: Earth and Planetary Science Letters, v. 382, p. 98–110, doi: 10.1016/j.epsl.2013.09.005.

Riedel, J.L., Clague, J.J., and Ward, B.C., 2010, Timing and extent of early marine oxygen isotope stage 2 alpine glaciation in Skagit Valley, Washington: Quaternary Research, v. 73, p. 313–323, doi: 10.1016/j.yqres.2009.10.004.

Rood, D.H., Burbank, D.W., and Finkel, R.C., 2011, Chronology of glaciations in the Sierra Nevada, California, from 10Be surface exposure dating: Quaternary Science Reviews, v. 30, p. 646–661, doi: 10.1016/j.quascirev.2010.12.001.

Rosenbaum, J.G., Reynolds, R.L., and Colman, S.M., 2012, Fingerprinting of glacial silt in lake sediments yields continuous records of alpine glaciation (35–15ka), western USA: Quaternary Research, v. 78, p. 333–340, doi: 10.1016/j.yqres.2012.06.004.

Rowan, A.V., Egholm, D.L., Quincey, D.J., and Glasser, N.F., 2015, Modelling the feedbacks between mass balance, ice flow and debris transport to predict the response to climate change of debris-covered glaciers in the Himalaya: Earth and Planetary Science Letters, v. 430, p. 427–438, doi: 10.1016/j.epsl.2015.09.004.

Russell, I.C., 1889, Quaternary history of Mono Valley, California: United States Geological Survey, p. 261-394 p.

Ryder, J.M., and Thomson, B., 1986, Neoglaciation in the southern Coast Mountains of British Columbia: chronology prior to the late Neoglacial maximum: Canadian Journal of Earth Sciences, v. 23, p. 273–287, doi: 10.1139/e86-031.

Saucedo, G.J., Little, J.D., Watkins, S.E., Davis, J.R., Mascorro, M.T., Walker, V.D., and Ford, E.W., 2005, Geologic map of the Lake Tahoe basin, California and Nevada: California Geological Survey.

Schaefer, J.M., Denton, G.H., Kaplan, M., Putnam, A., Finkel, R.C., Barrell, D.J., Andersen, B.G., Schwartz, R., Mackintosh, A., Chinn, T., and others, 2009, High-frequency Holocene glacier fluctuations in New Zealand differ from the northern signature: science, v. 324, p. 622–625.

Schaefer, J.M., Putnam, A.E., Denton, G.H., Kaplan, M.R., Birkel, S., Doughty, A.M., Kelley, S., Barrell, D.J.A., Finkel, R.C., Winckler, G., Anderson, R.F., Ninneman, U.S., Barker, S., Schwartz, R., et al., 2015, The Southern Glacial Maximum 65,000 years ago and its Unfinished Termination: Quaternary Science Reviews, v. 114, p. 52–60, doi: 10.1016/j.quascirev.2015.02.009.

Shakesby, R.A., 1997, Pronival (protalus) ramparts: a review of forms, processes, diagnostic criteria and p alaeoenvi ronmental implications: Progress in Physical Geography, v. 21, p. 394–418, doi: 10.1177/030913339702100304.

Sharp, R.P., and Birman, J.H., 1963, Additions to classical sequence of Pleistocene glaciations, Sierra Nevada, California: Geologic Society of America Bulletin, v. 74, p. 1079–1086.

Snowball, I., 1993, Mineral magnetic properties of Holocene lake sediments and soils from the Kårsa valley, Lappland, Sweden, and their relevance to palaeoenvironmental reconstruction: Terra Nova, v. 5, p. 258–270, doi: 10.1111/j.1365-3121.1993.tb00257.x.

Solomina, O.N., Bradley, R.S., Hodgson, D.A., Ivy-Ochs, S., Jomelli, V., Mackintosh, A.N., Nesje, A., Owen, L.A., Wanner, H., Wiles, G.C., and Young, N.E., 2015, Holocene glacier fluctuations: Quaternary Science Reviews, v. 111, p. 9–34, doi: 10.1016/j.quascirev.2014.11.018.

Stock, G., and Anderson, R., 2012, FINAL REPORT December 2012:, http://www.cfc.umt.edu/cesu/Reports/NPS/CU/2009/09_11Anderson_YOSE_glaciers_fnl%20rpt.pdf (accessed October 2015).

Stock, G.M., Anderson, R.S., and Devine, P., 2013, Retreat and stagnation of Little Ice Age glaciers in Yosemite National Park: Abstracts with Programs - Geological Society of America, v. 45, p. 53–53.

Stuiver, M., and Reimer, P.J., 1993, Extended 14C Data Base and Revised CALIB 3.0 14C Age Calibration Program: Radiocarbon, v. 35, p. 215–230, doi: 10.1017/S0033822200013904.

Wershow, H.N., 2016, A Holocene Glaciolacustrine Record of the Lyman Glacier and Implications for Glacier Fluctuations in the North Cascades, Washington [MS]: Western Washington University, 89 p.

Whiting, J.D., 1985, Late Pleistocene and Holocene glacial history of the Pyramid Creek-South Fork American River drainage, Sierra Nevada, California [M.S. thesis]: California State University, 162 p.

Wiles, G.C., Jacoby, G.C., Davi, N.K., and McAllister, R.P., 2002, Late Holocene glacier fluctuations in the Wrangell Mountains, Alaska: Geological Society of America Bulletin, v. 114, p. 896–908, doi: 10.1130/0016-7606(2002)114<0896:LHGFIT>2.0.CO;2.

Wiles, G.C., Lawson, D.E., Lyon, E., Wiesenberg, N., and D'Arrigo, R.D., 2011, Tree-ring dates on two pre-Little Ice Age advances in Glacier Bay National Park and Preserve, Alaska, USA: Quaternary Research, v. 76, p. 190–195, doi: 10.1016/j.yqres.2011.05.005.

Wood, S.H., 1977, Distribution, correlation, and radiocarbon dating of late Holocene tephra, Mono and Inyo craters, eastern California: Geological Society of America Bulletin, v. 88, p. 89–95.

Wright Jr., H.E., 1967, A square-rod piston sampler for lake sediments: Journal of Sediment Petrology, v. 37, p. 975–976.

Zimmerman, S.H., 2014, High-precision 10Be dating of late Holocene glaciation in the Sierra Nevada: Testing hypotheses of the Little Ice Age and Holocene climate change: Lawrence Livermore National Laboratory, 1–17 p.

8.0 Tables

Table 1. Radiocarbon ages from lake sediment cores below the Lyell and Maclure glaciers in Yosemite National Park.

Sample ID	Lab Code [1]	Depth (cm) [2]	Material	^{14}C Age (yr BP)	Median Age (cal yr BP)	2σ age range (cal yr BP)
LL16-C-01	176286	22	Bulk	1475 ± 40	1362	1416-1297
LL16-C-02	176287	44	Bulk	1895 ± 30	1844	1897-1735
LM16-C-01	176288	25	Bulk	1730 ± 45	1643	1738-1537
LM16-C-02	176289	65	Bulk	2875 ± 40	3002	3081-2879
LM16-C-03	176290	92	Bulk	5075 ± 35	5818	5828-5754

[1] Radiocarbon samples analyzed at the LLNL CAMS facility, Livermore, CA
[2] Depth below the sediment surface

Table 2. Tephrochronology from lake sediment cores below the Lyell and Maclure glaciers using electron microprobe analysis (EMA).

Sample ID	Tephra	Depth (cm)	Identification method	Age (yr BP)	± yr	Calibrated age (cal yr BP) [1]
LL16-T-01	Mono	42	EMA	~1,950 - 795	-	-
LL16-T-02	Tsoyowata	136	EMA	7014	80	7,740 - 7950
LM16-T-01	Mono	43	EMA	~1,950 - 795	-	-

[1] Calibrated age from Bacon (1983)

Table 3. Maximum Neoglacial and modern glacier surface area extent as well as the respective decrease in extent from Neoglacial to Modern.

Glacier	Area of glacial extent (km^2)	Decrease in glacial extent (%)
Maclure (Neoglacial)	0.329	-
Maclure (modern)	0.140	57.4
West Lyell (Neoglacial)	0.456	-
West Lyell (modern)	0.244	46.5
East Lyell (Neoglacial)	0.653	-
East Lyell (modern)	0.048	92.6
Price E (Neoglacial)	0.037	-
Price E (modern)	0.000	100
Price C (Neoglacial)	0.023	-
Price C (modern)	0.000	100
Price W1 (Neoglacial)	0.117	-
Price W1 (modern)	0.000	100
Price W2 (Neoglacial)	0.024	-
Price W2 (modern)	0.000	100

9.0 Figures

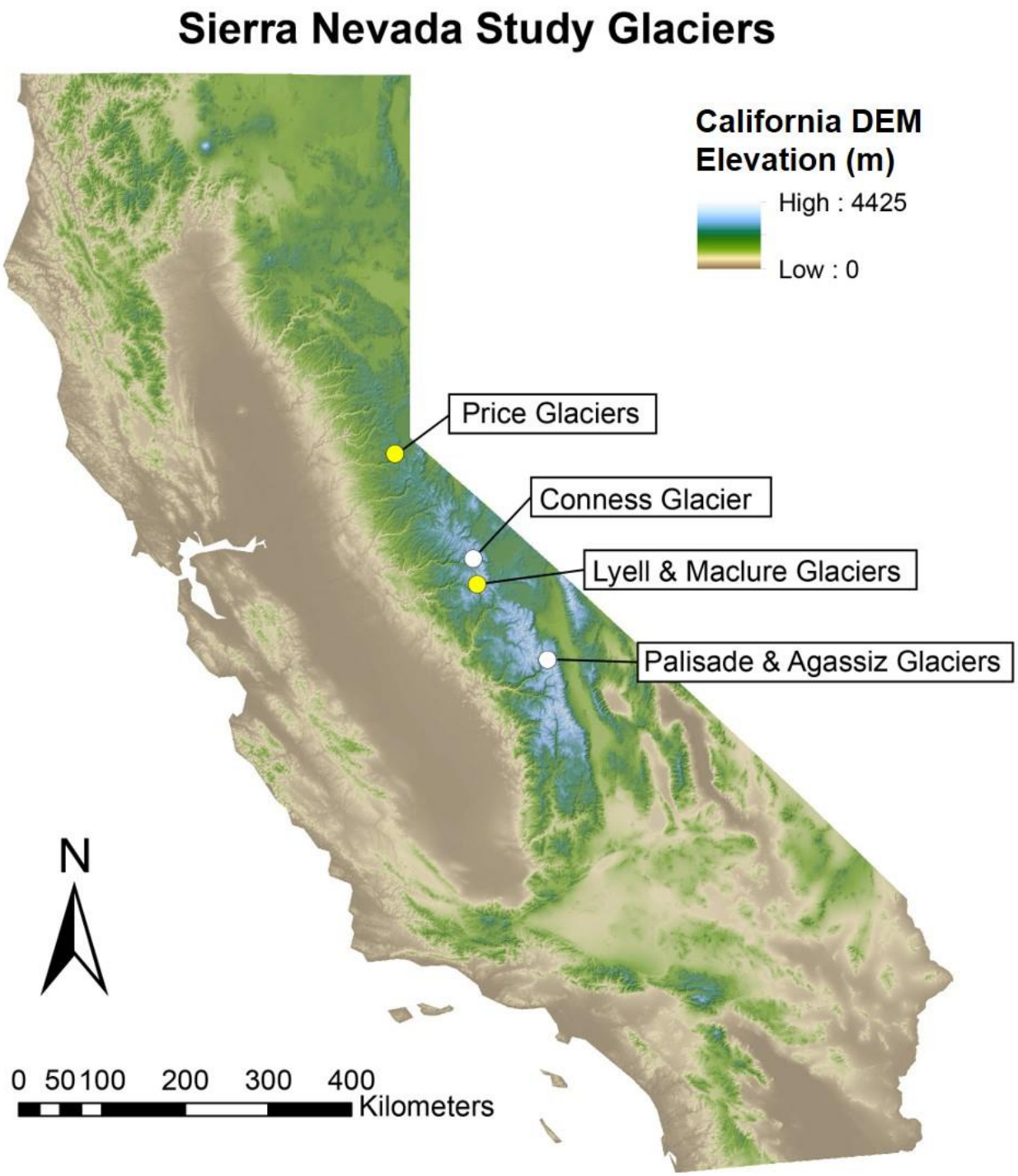

Figure 1. Location map of Sierra Nevada field sites. Lake coring sites for this study are indicated by yellow circles. White circles indicate the other ^{10}Be CRN sampling sites of Clark et al. (2015).

Figure 2. Photographs of the (a) Lyell terminal Neoglacial moraine and upper lake, (b) Desolation terminal Neoglacial moraine, and (c) Maclure terminal Neoglacial moraine. All are fresh, sharp crested with steep sides, boulder covered, and lacking vegetation.

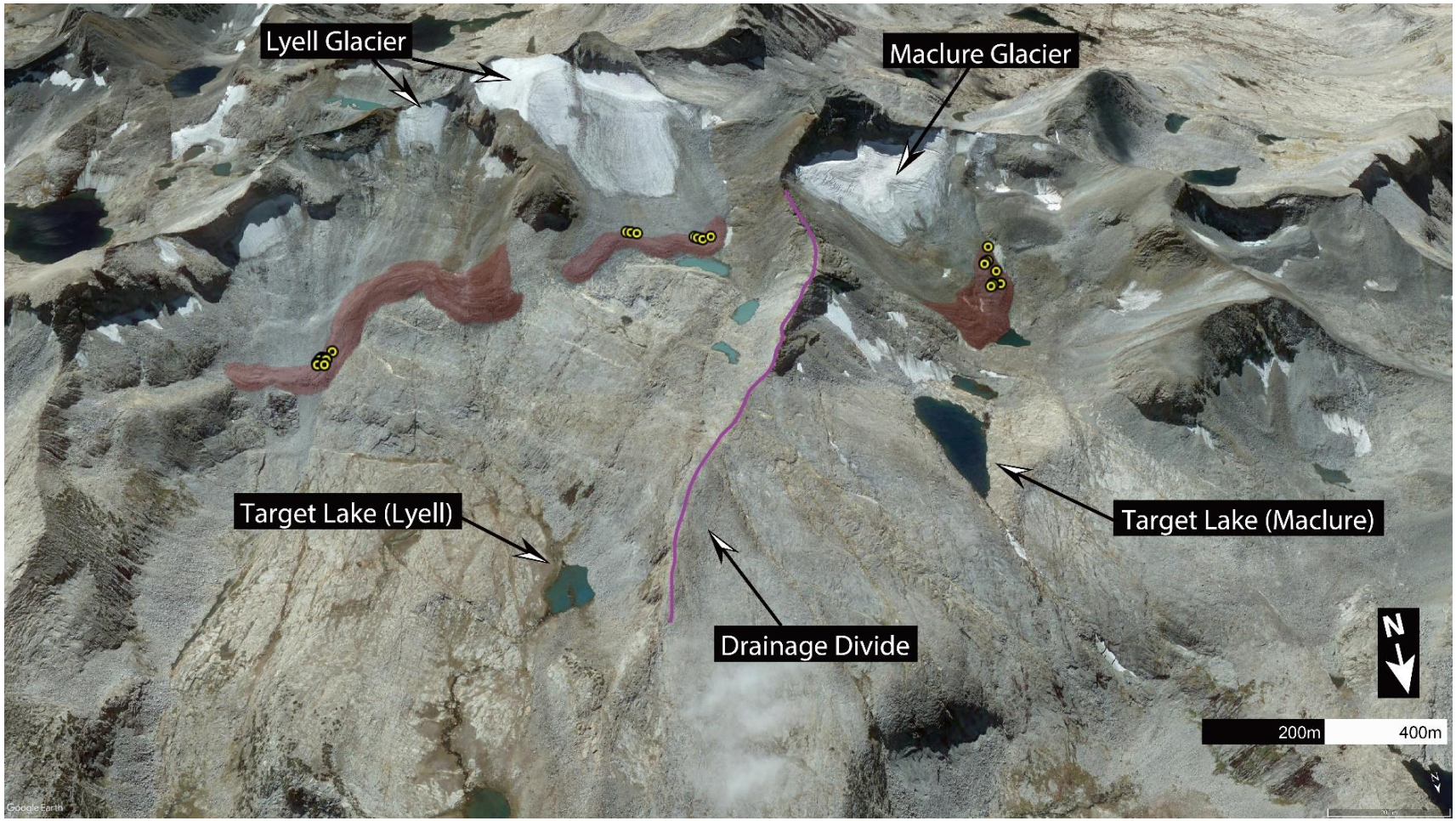

Figure 3. Aerial imagery of the Yosemite field sites indicating primary targets for lake coring (all in glacial melt-water streams). Red fill highlights Neoglacial moraines and yellow dots indicate ^{10}Be CRN sample sites on terminal moraines of Maclure Glacier and both lobes of the Lyell Glacier. Imagery taken from 9/14/2013 (Google Earth).

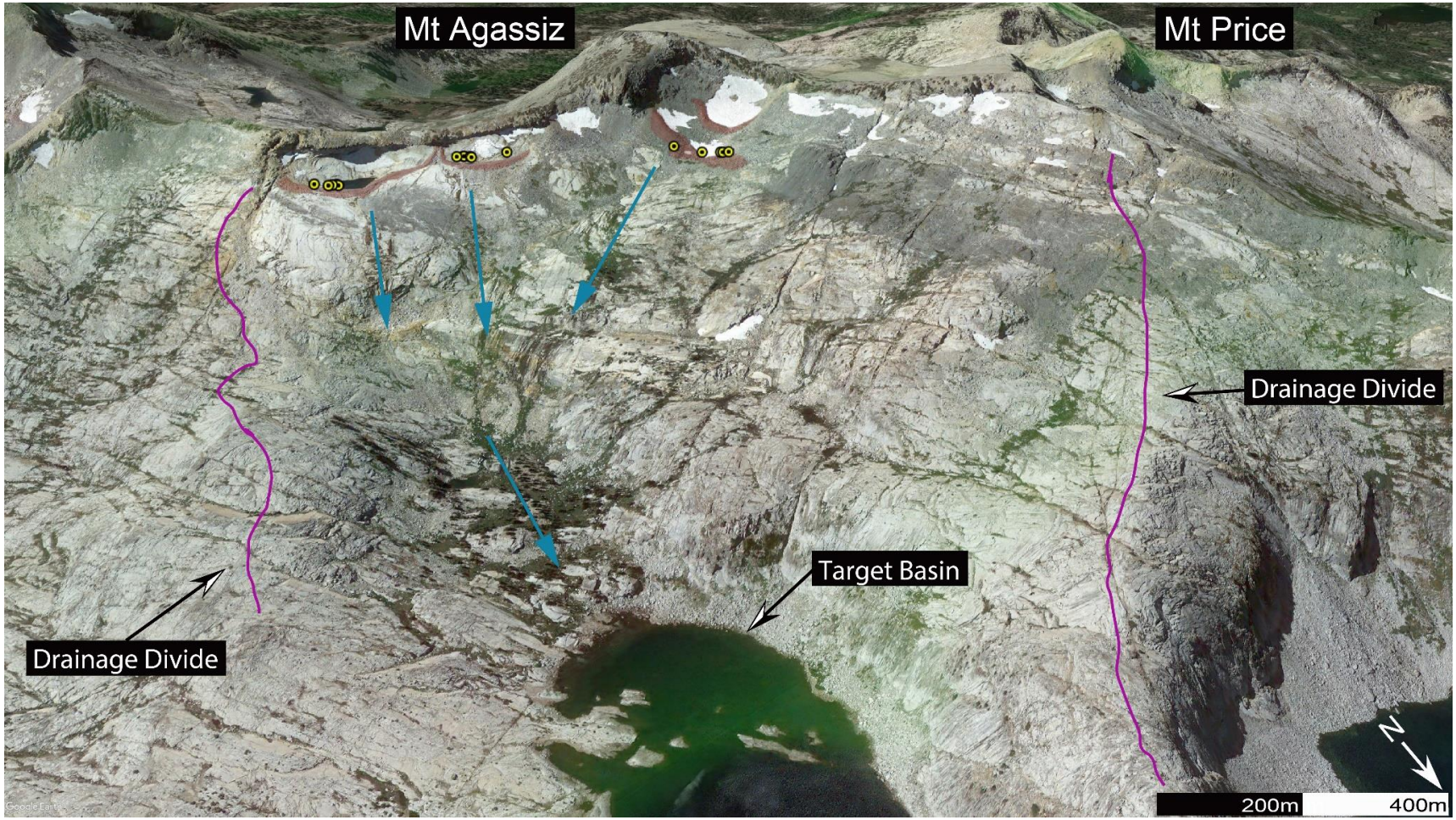

Figure 4. Aerial imagery of the Desolation field site indicating primary target for lake coring in downstream of the Price Glaciers. Red fill highlights Neoglacial moraines and yellow dots indicate ^{10}Be CRN sample sites. Blue arrows indicate general flow direction from each moraine. Imagery taken from 8/28/2012 (Google Earth).

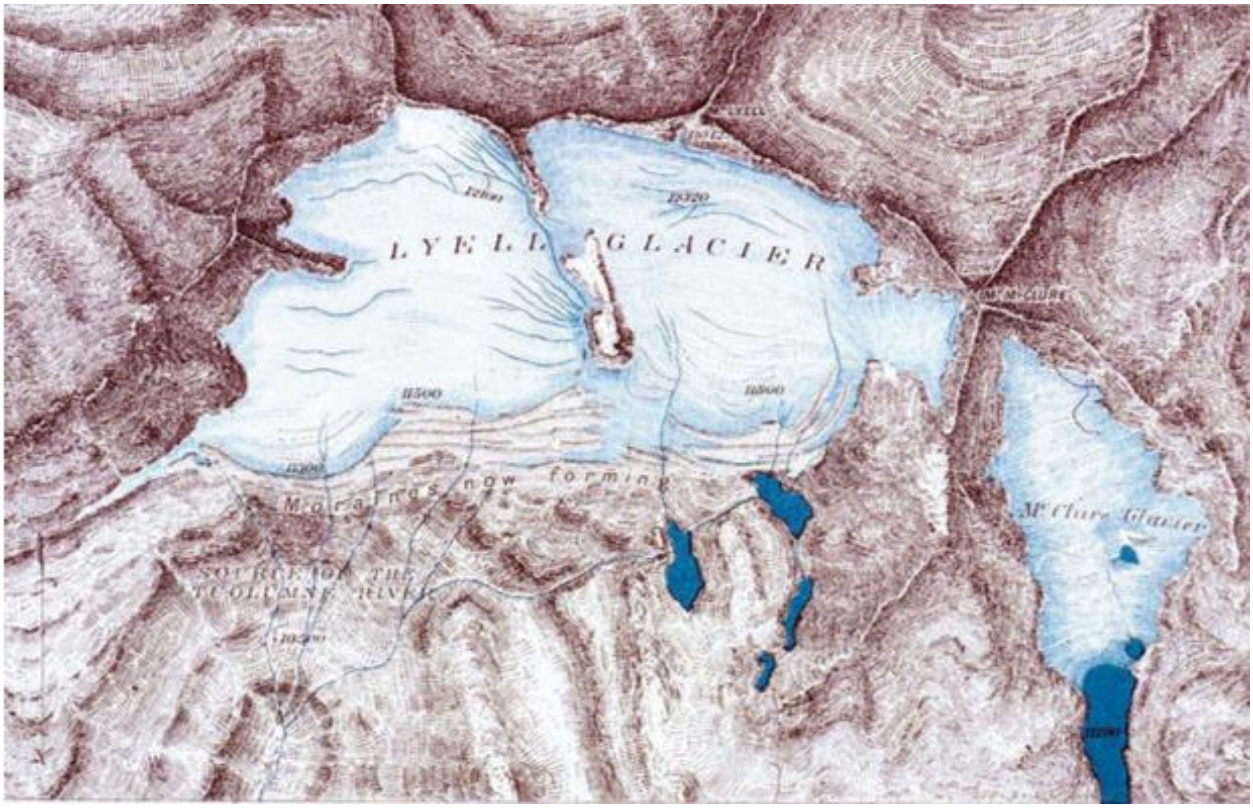

Figure 5. Map of the Lyell and Maclure glaciers in Yosemite National Park as they appeared in 1883. This map was created by W.D. Johnson and published in Russell (1889).

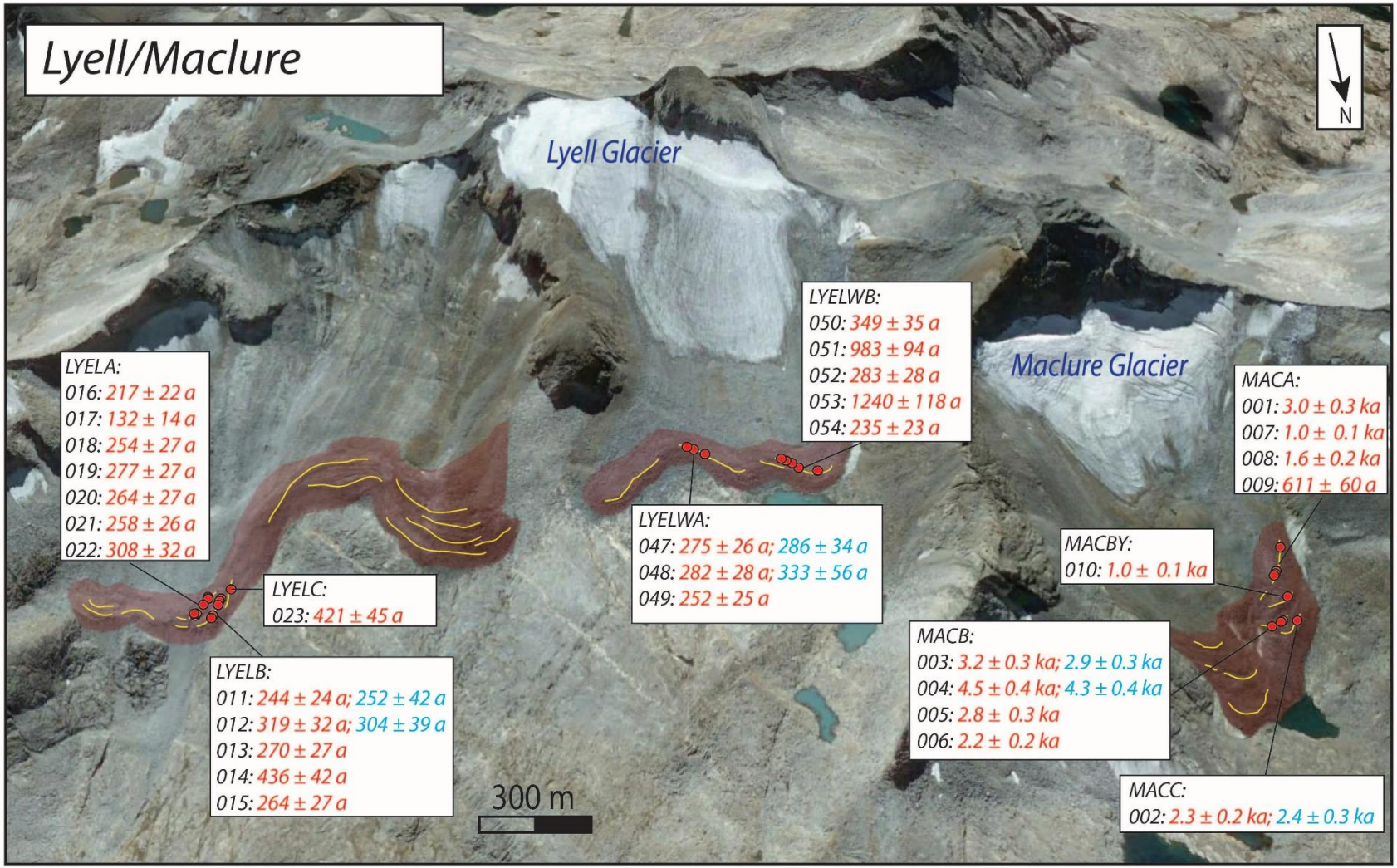

Figure 6. CRN exposure ages displayed for the associated boulders along each moraine sequence of the Lyell Glacier and Maclure Glacier in Yosemite National Park. Red text indicates ^{10}Be ages and blue text represents ^{26}Al CRN ages. Moraine crests are shown by yellow lines and sampled boulder locations are shown by red dots. Figure by Alan Hidy.

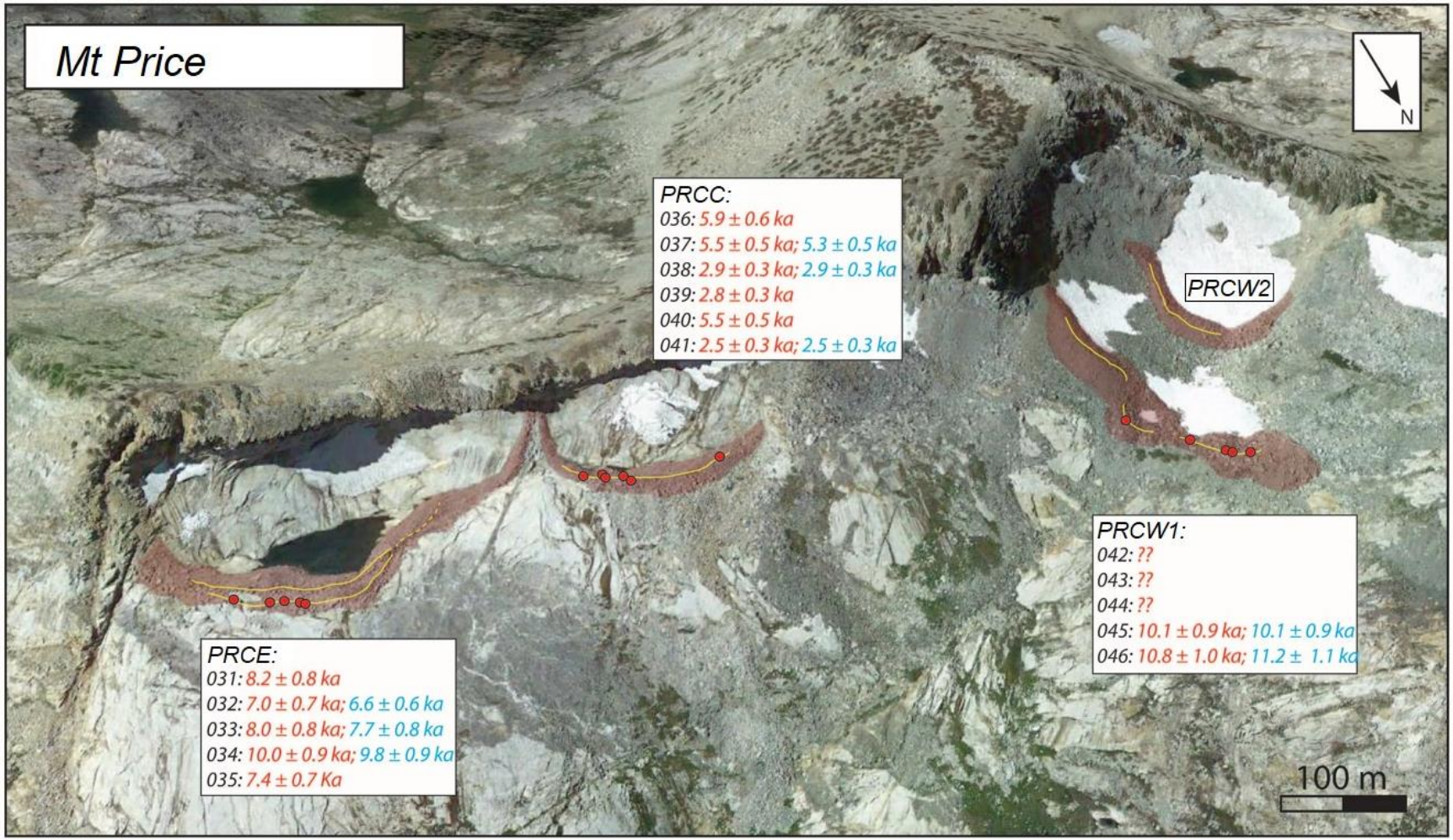

Figure 7. CRN ages are displayed along each moraine sequence of the Price glaciers in the Desolation Wilderness. Red text indicates ^{10}Be ages and blue text represents ^{26}Al CRN ages. Moraine crests are shown by yellow lines and sampled boulder locations are shown by red dots. Figure by Alan Hidy.

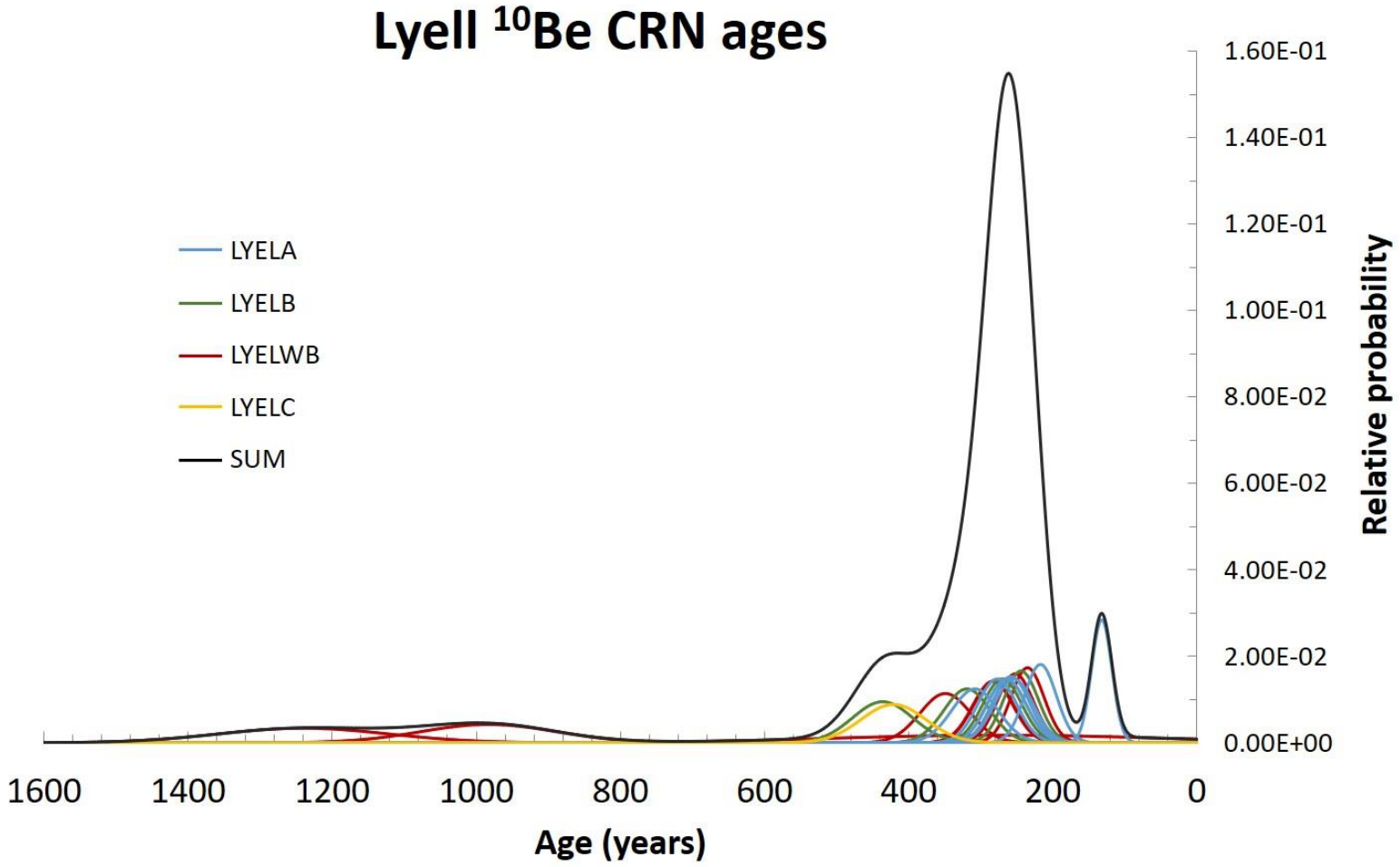

Figure 8. Camel diagram of ^{10}Be CRN ages and 1-sigma uncertainty from the Lyell Glacier in Yosemite National Park. Each moraine and/or distinct ridge is shown in a different color (refer to Figure 6 for reference).

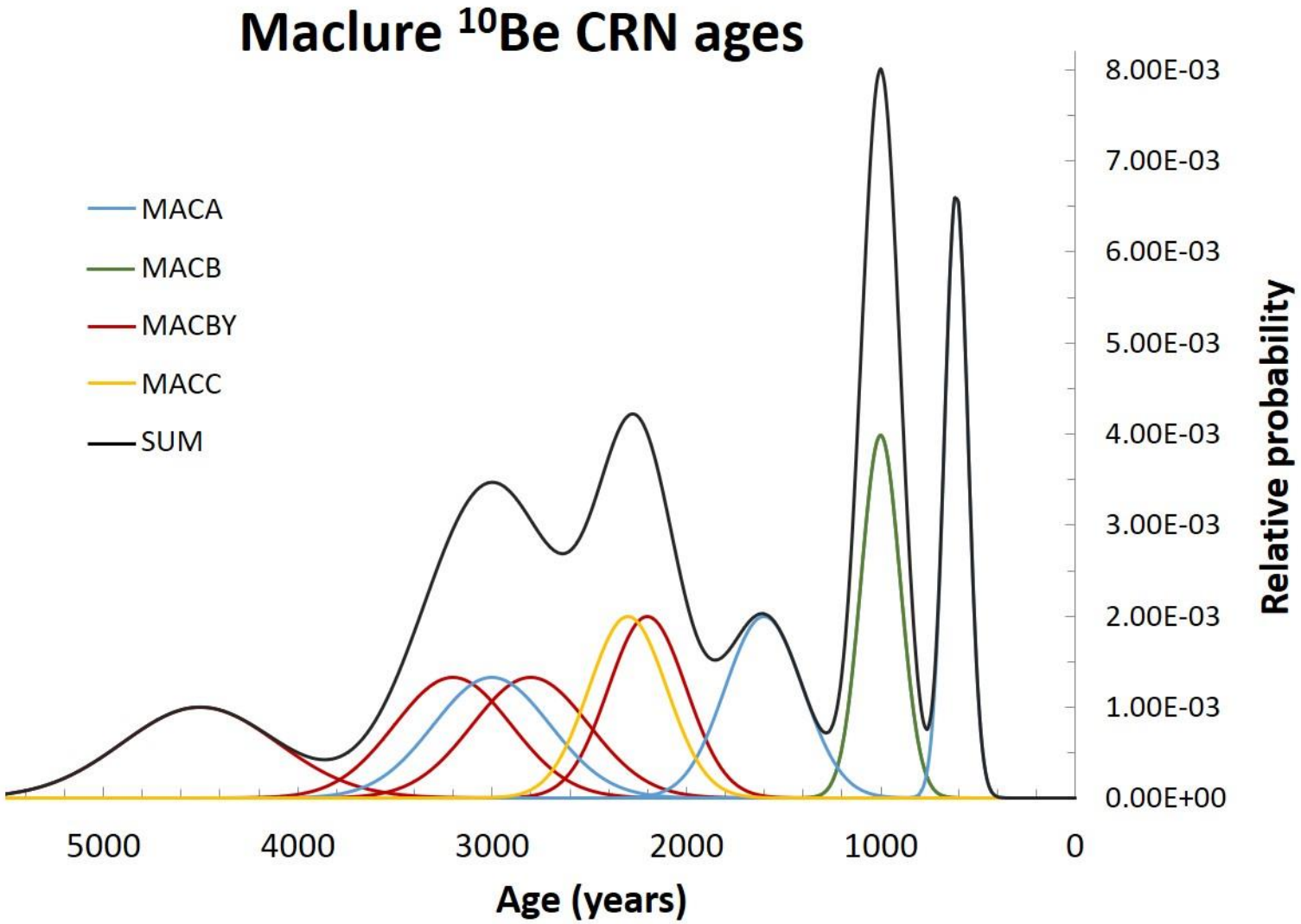

Figure 9. Camel diagram of ^{10}Be CRN ages and 1-sigma uncertainty from the Maclure Glacier in Yosemite National Park. Each moraine and/or distinct ridge is shown in a different color (refer to Figure 6 for reference).

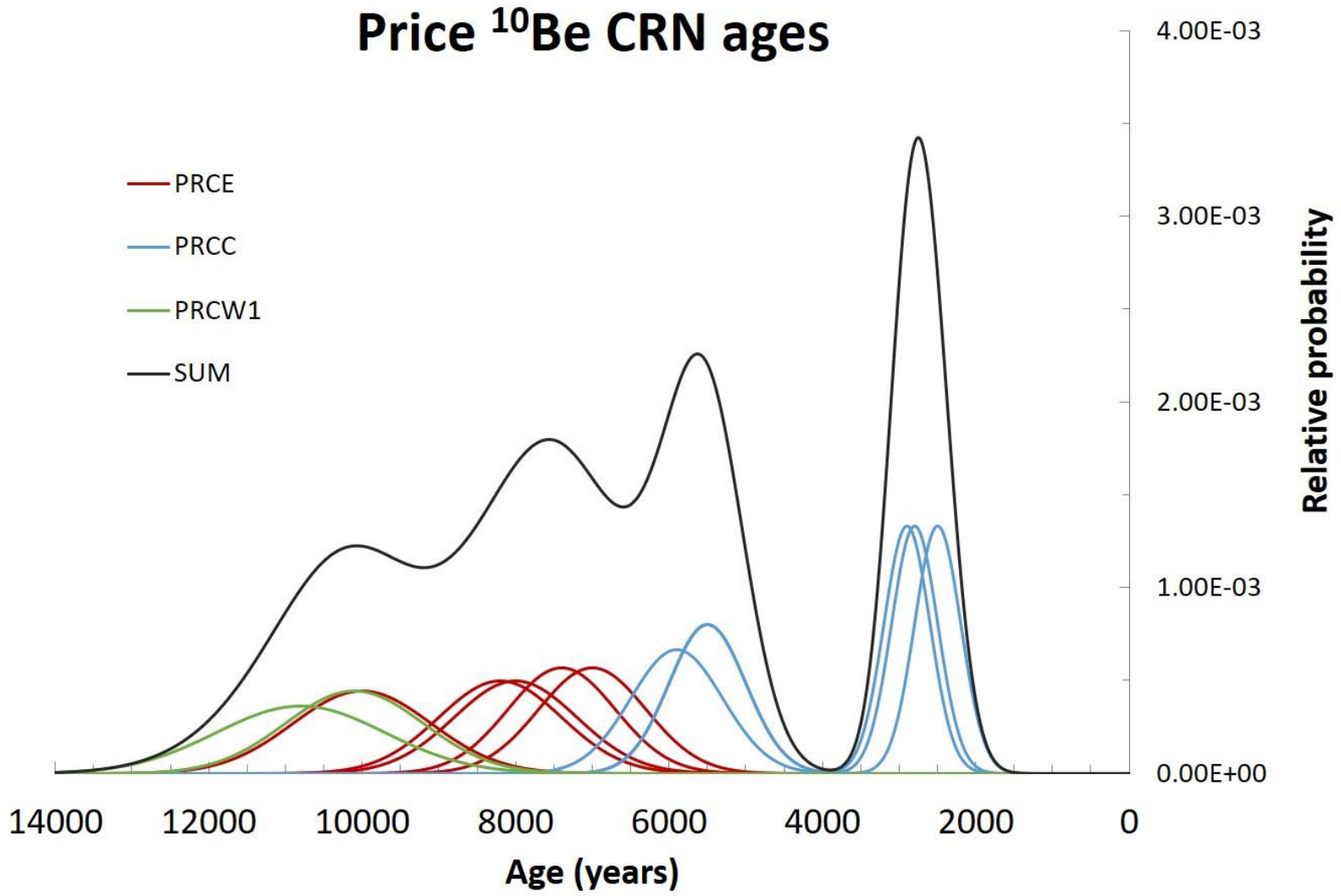

Figure 10. Camel diagram of ^{10}Be CRN ages and 1-sigma uncertainty from the extinct glaciers beneath Mt Price in the Desolation Wilderness. Each moraine is shown in a different color (refer to Figure 7 for reference).

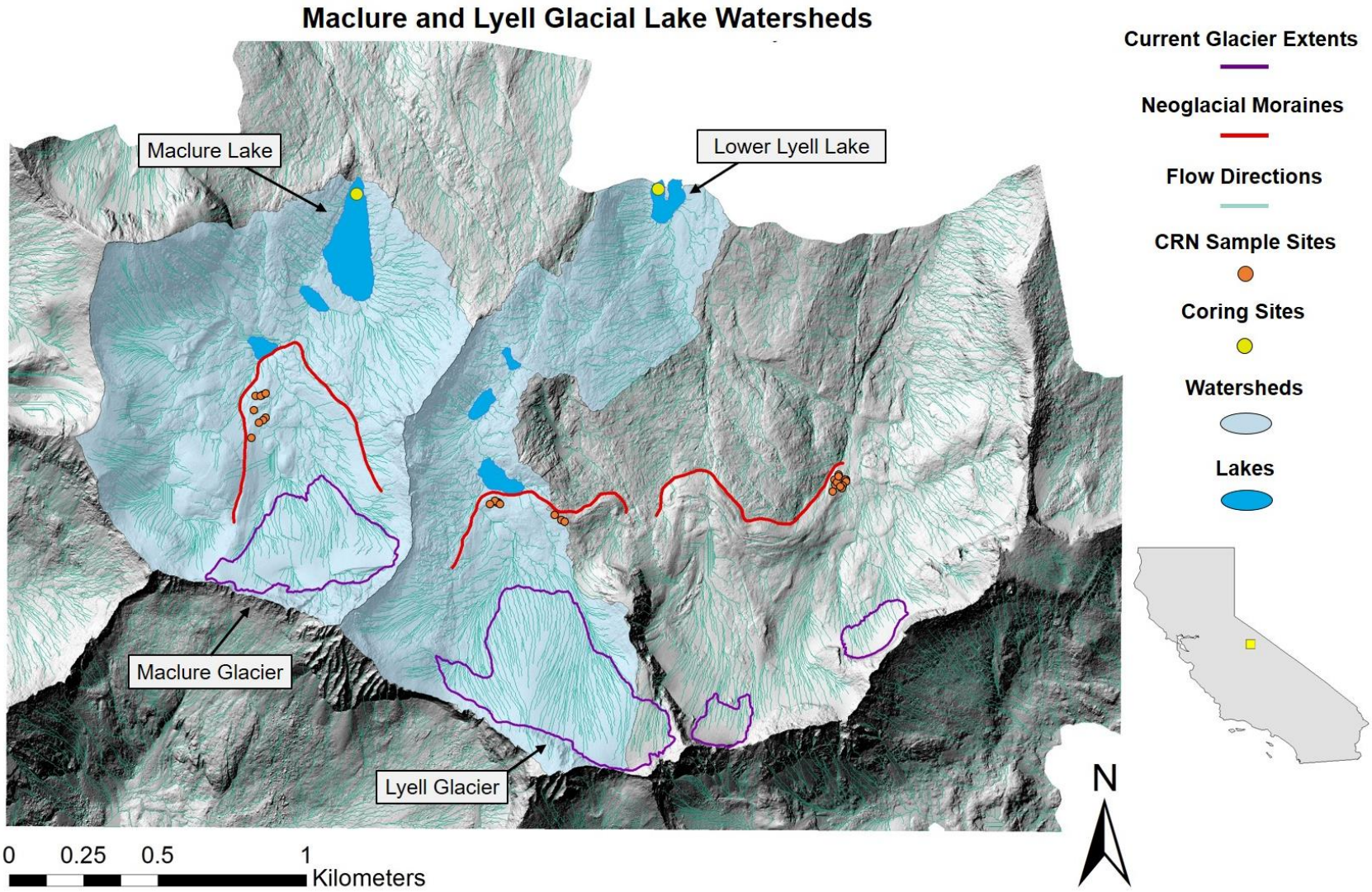

Figure 11. Lyell and Maclure study lake watersheds are filled in with light blue over a hillshade created from the 2007 lidar DEM data. The Neoglacial moraine of the western lobe of the Lyell glacier is divided into two separate watersheds.

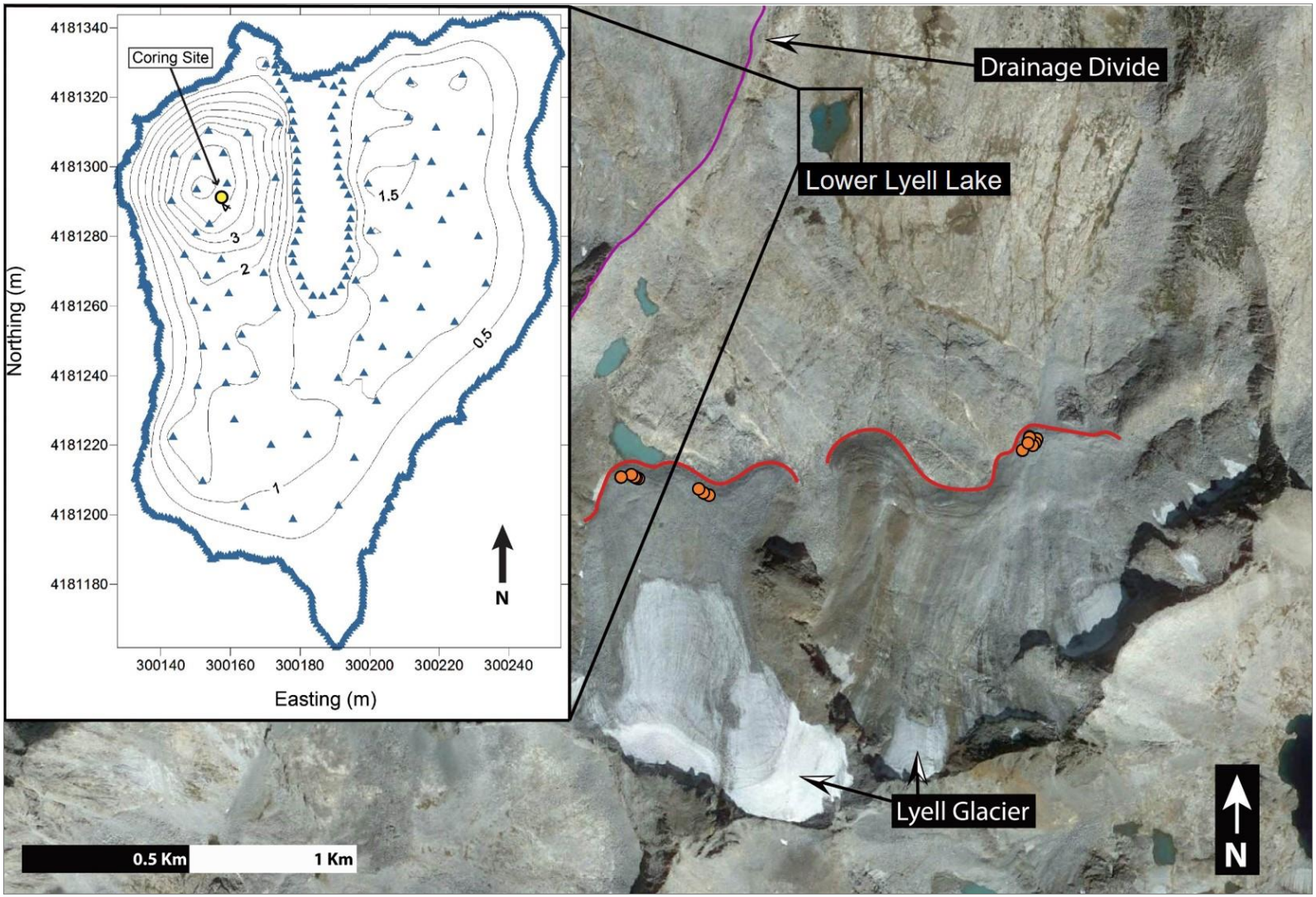

Figure 12. Aerial imagery of the Lyell Glacier and respective drainage. Red lines indicate the maximum Neoglacial extents and orange dots indicate ^{10}Be CRN sample sites on terminal moraines. Inset map illustrates Lower Lyell Lake bathymetry based off depth measurements (shown by blue triangles). Contour lines display 0.5 m intervals. Imagery taken from 9/14/2013 (Google Earth).

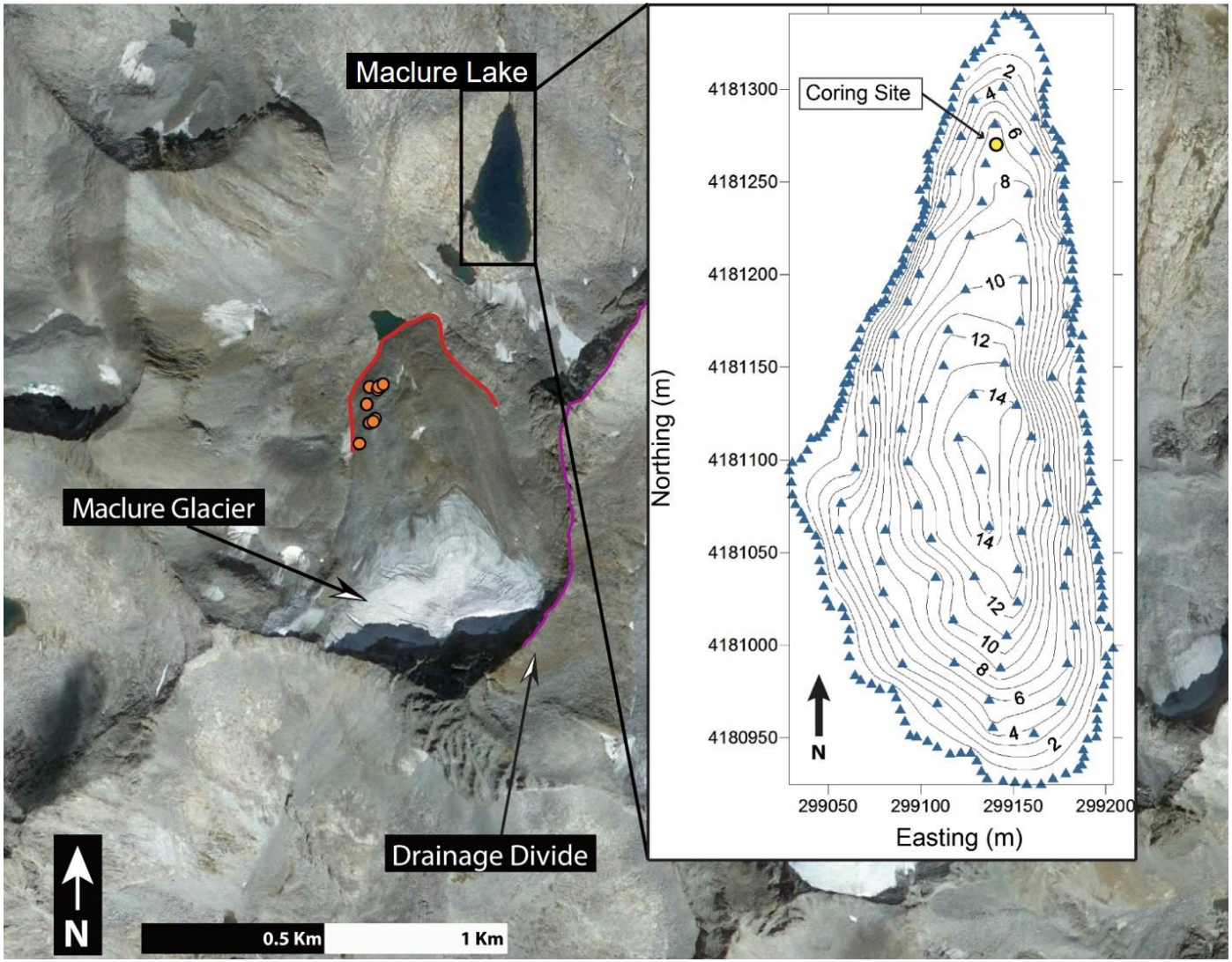

Figure 13. Aerial imagery of the Maclure glacier and respective drainage. Red lines indicate the maximum Neoglacial extents and orange dots indicate ^{10}Be CRN sample sites on terminal moraines. Inset map illustrates Maclure Lake bathymetry based off depth measurements (shown by blue triangles). Contour lines display 1 m intervals. Imagery taken from 9/14/2013 (Google Earth).

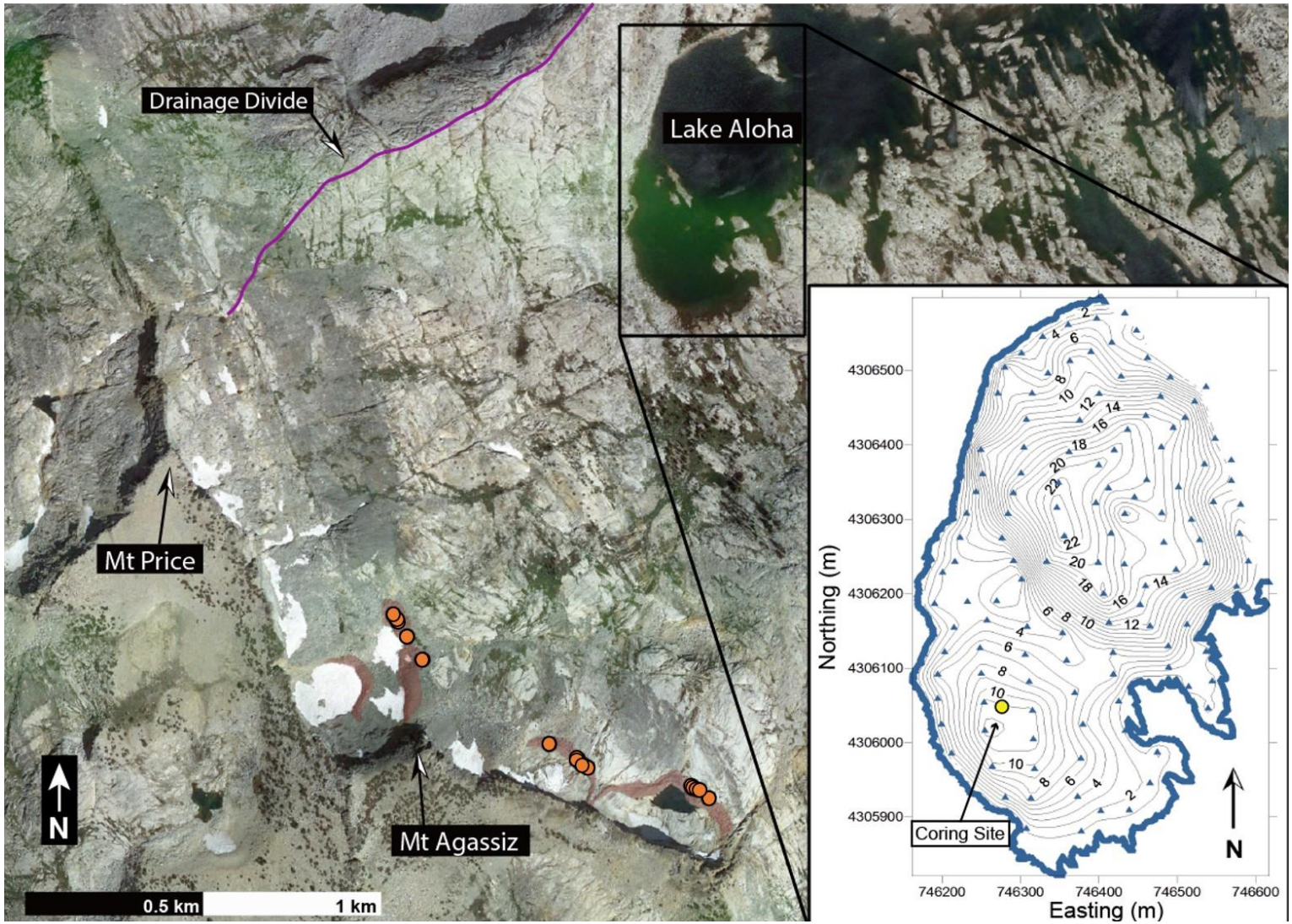

Figure 14. Imagery of the Price glaciers and respective drainage. Red fill highlights Neoglacial moraines and orange dots indicate ^{10}Be CRN sample sites on terminal moraines. Inset map illustrates Lake Aloha bathymetry based off depth measurements (shown by blue triangles). Contour lines display 1m intervals. Imagery taken from 8/2012 (Google Earth).

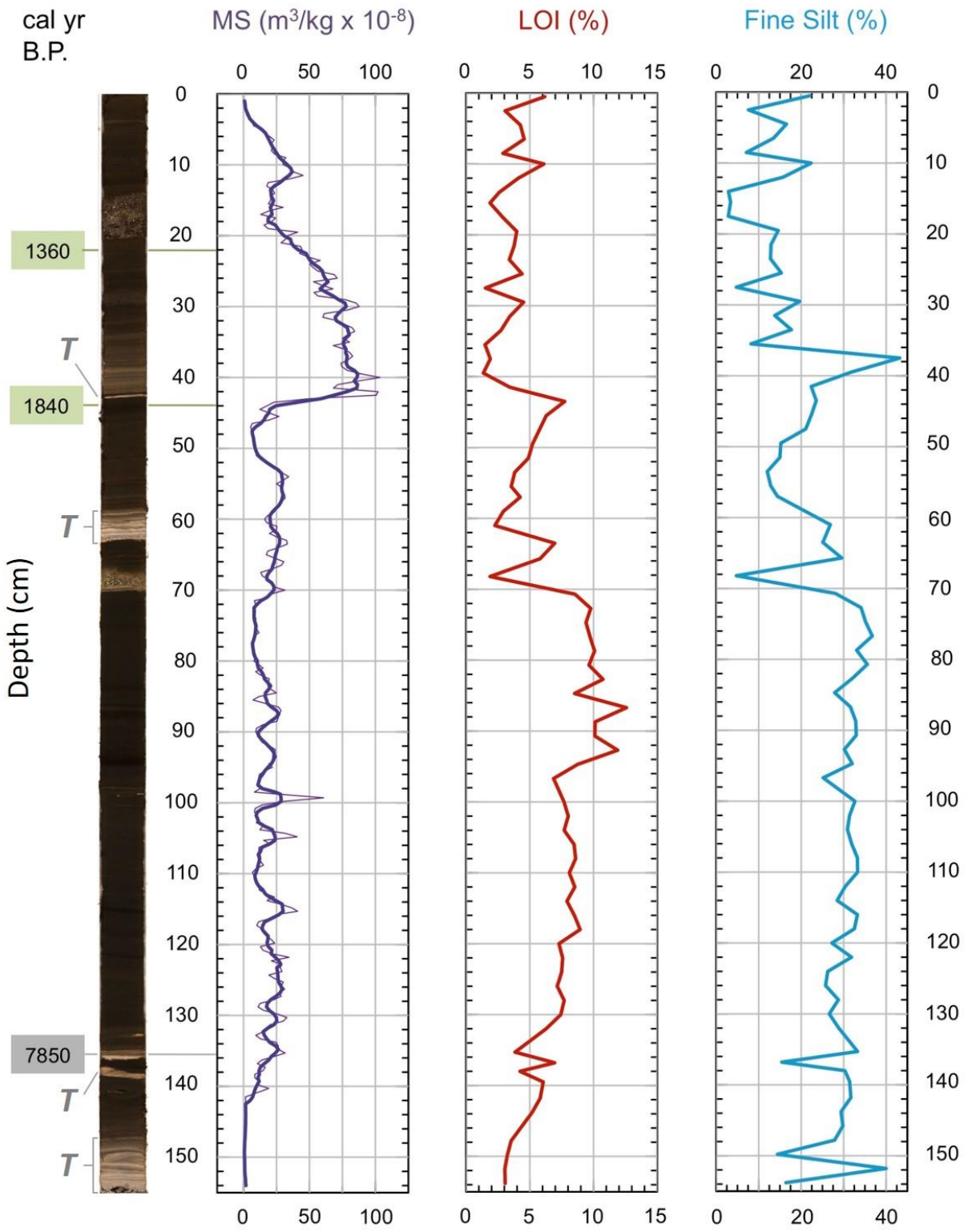

Figure 15. Sediment core LL16-01-01/02/03/04 (composite core record) from Lower Lyell Lake with rock flour proxies MS, LOI, and fine silt %. MS data is displayed in 0.5 cm measurements (light, thin purple line) and a five-point running average (dark, thick purple line). Grey 'T's indicate tephra deposits. Median cal yr BP ages are shown for bulk radiocarbon (green) and tephra (grey).

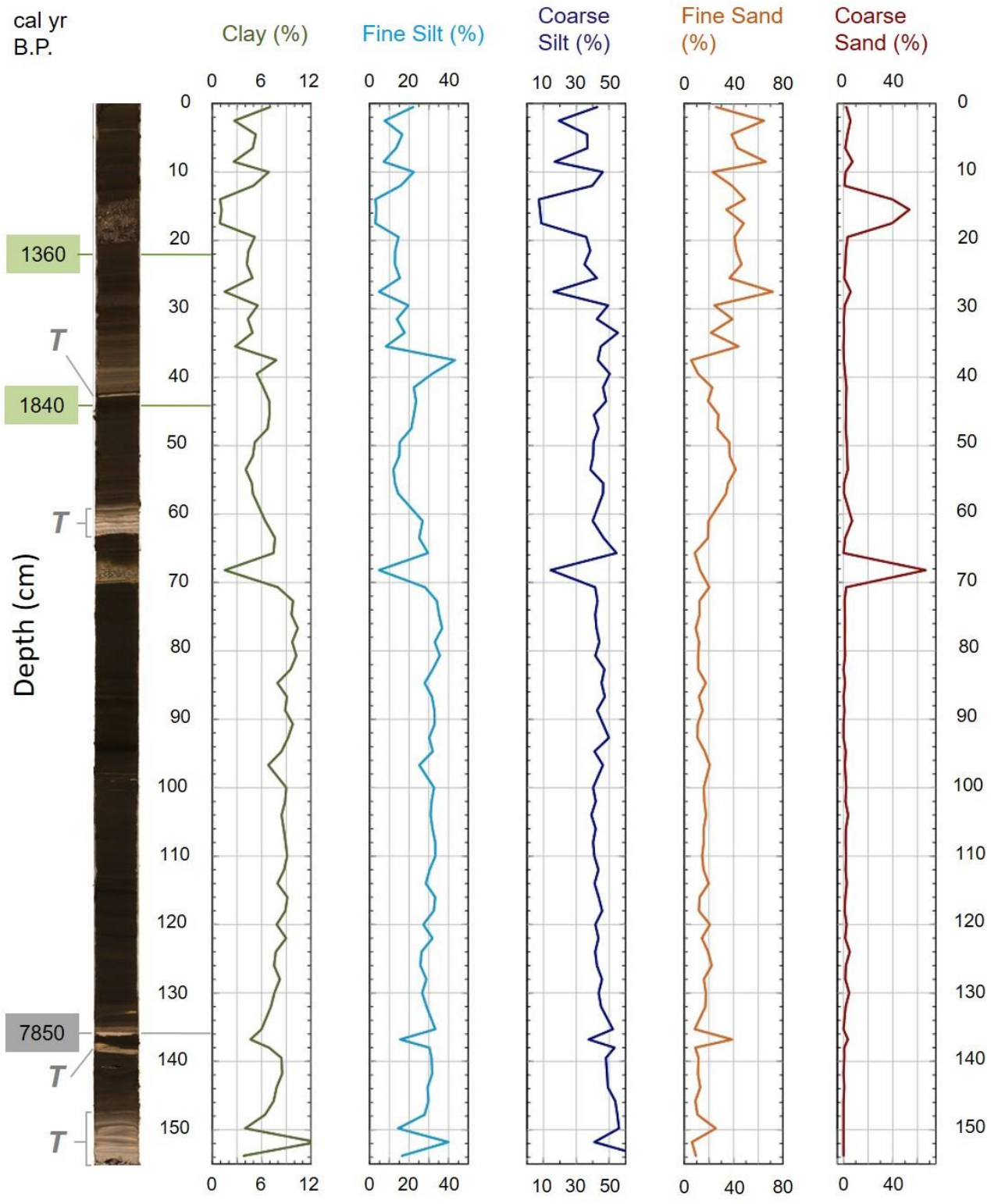

Figure 16. Sediment core LL16-01-01/02/03/04 (composite core record) from Lower Lyell Lake with grain size distribution of clastic sediments. Grey 'T's indicate tephra deposits. Median cal yr BP ages are shown for bulk radiocarbon (green) and tephra (grey).

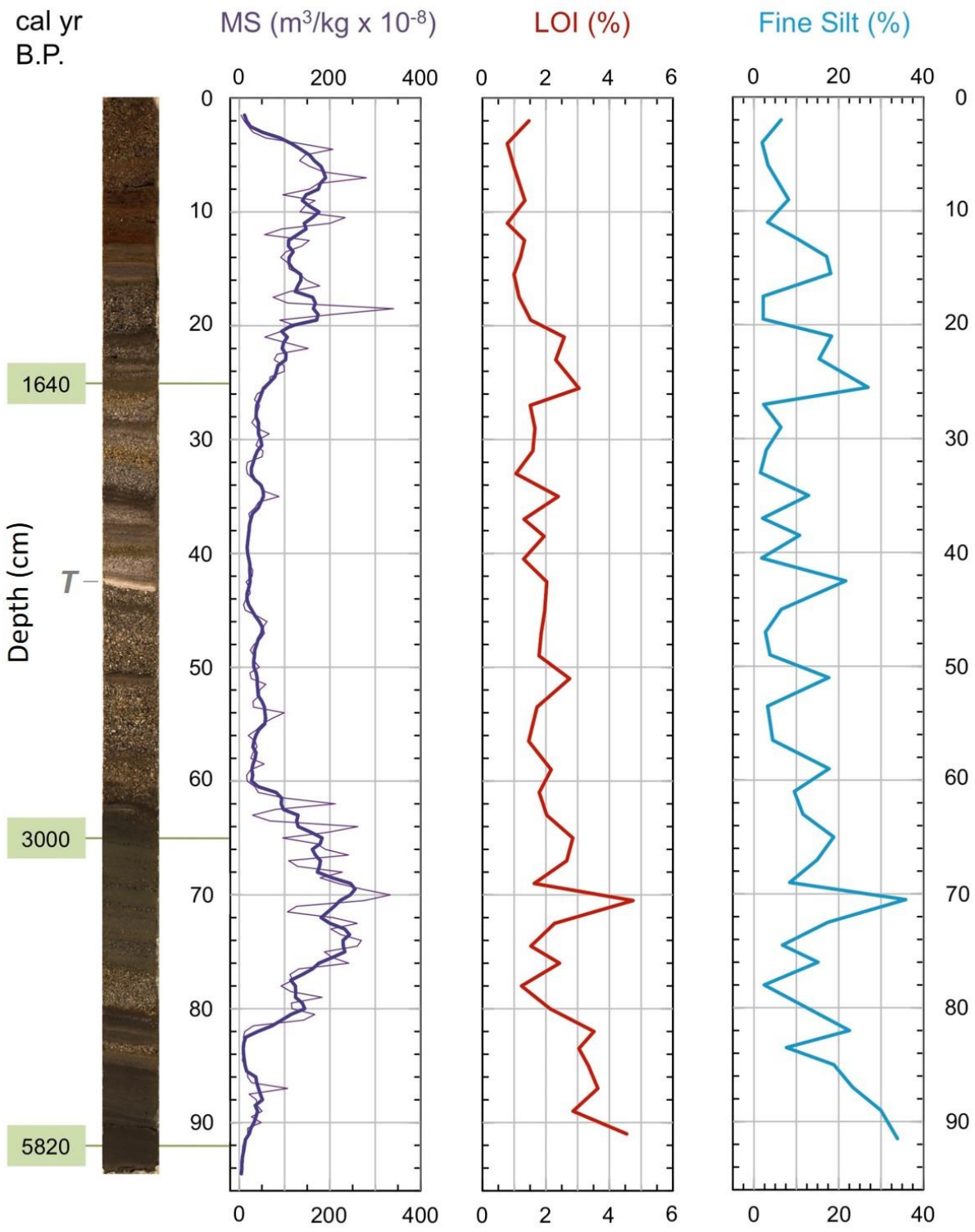

Figure 17. Sediment core LM16-01-01 from Maclure Lake with rock flour proxies MS, LOI, and fine silt %. MS data is displayed in 0.5 cm measurements (light, thin purple line) and a five-point running average (dark, thick purple line). Grey 'T's indicate tephra deposits. Median cal yr BP ages are shown for bulk radiocarbon (green) and tephra (grey).

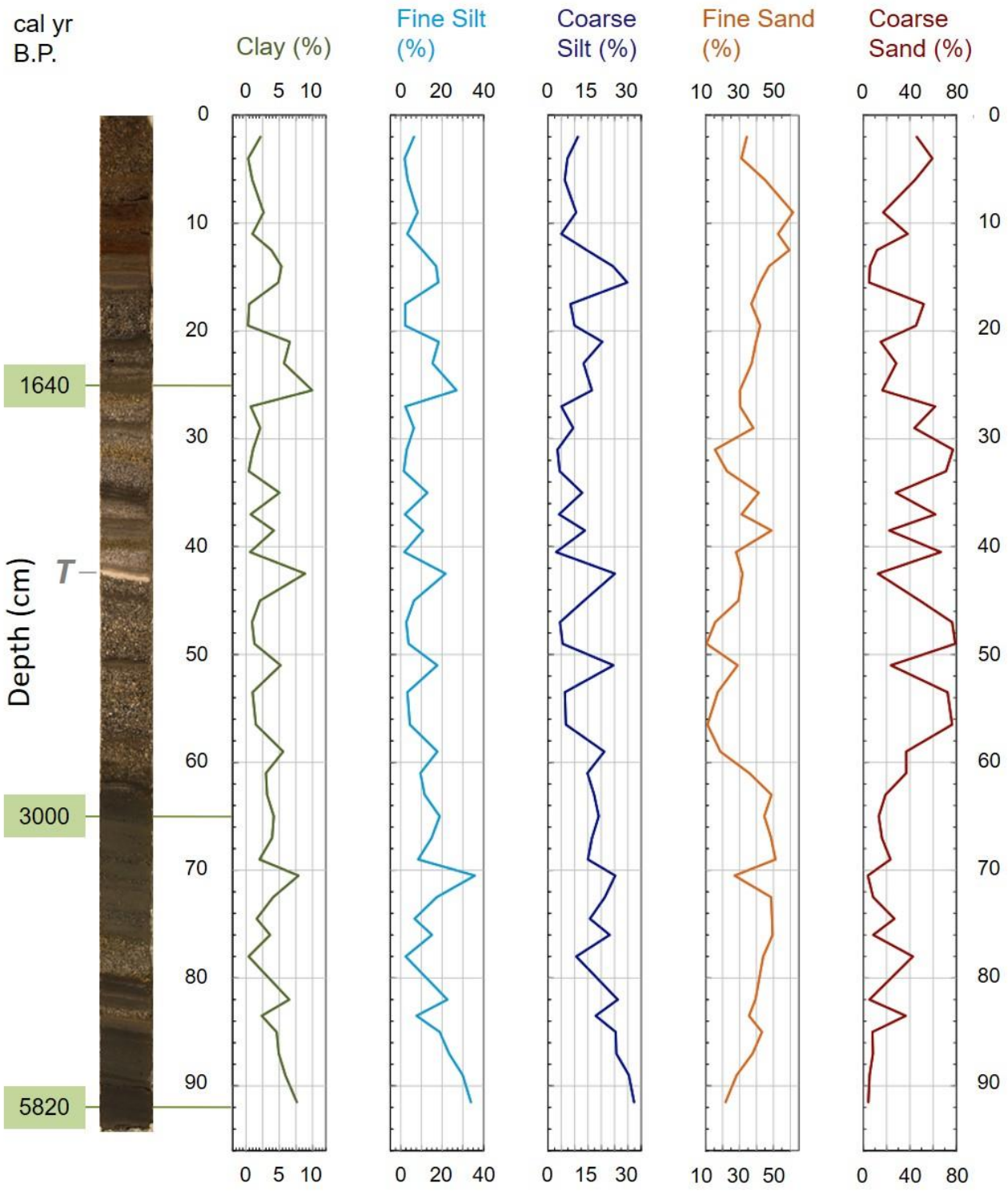

Figure 18. Sediment core LM16-01-01 from Maclure Lake with grain size distribution of clastic sediments. Grey 'T's indicate tephra deposits. Median cal yr BP ages are shown for bulk radiocarbon (green) and tephra (grey).

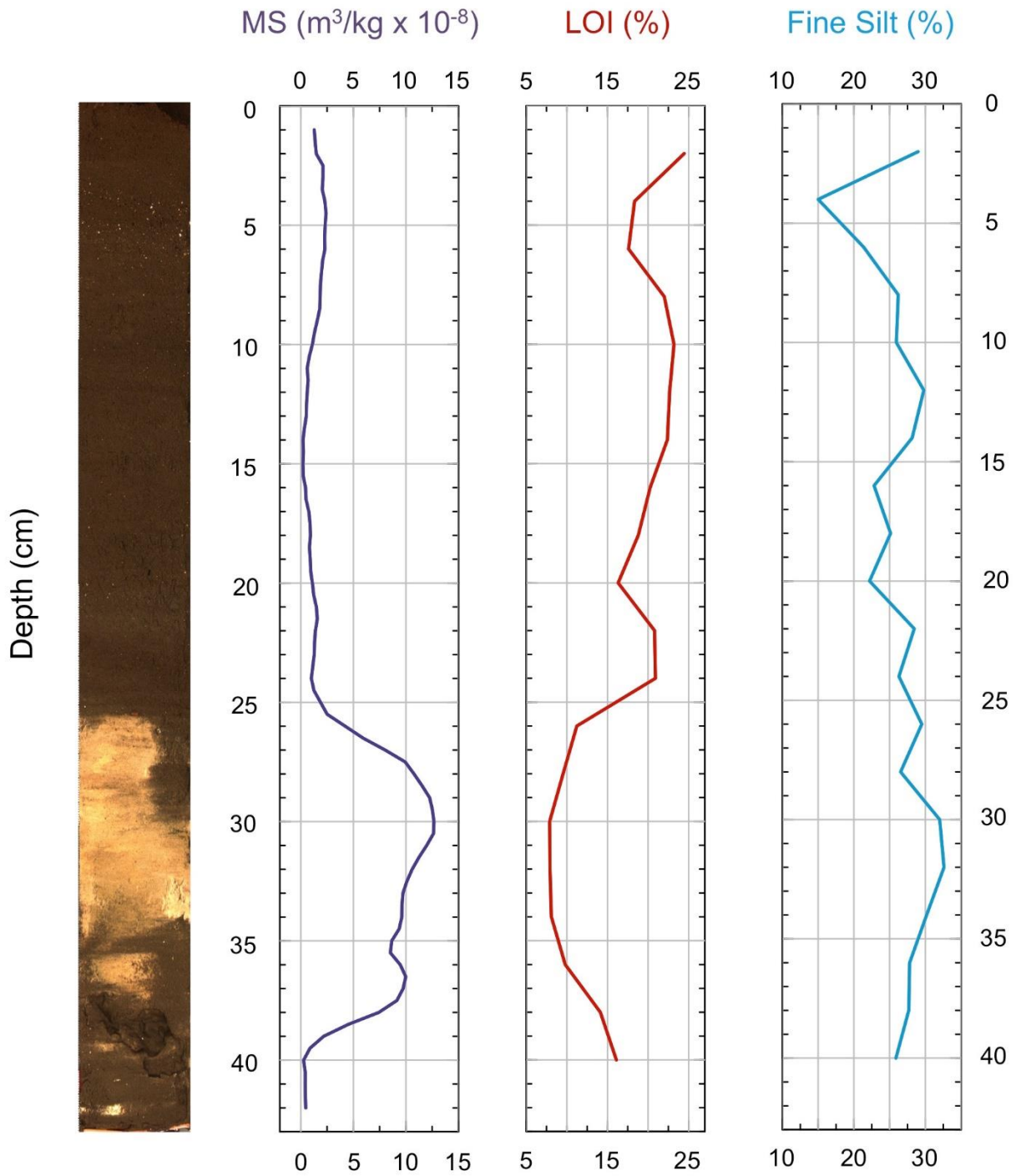

Figure 19. Sediment core LA16-G02 from Lake Aloha below the presumed Price glaciers with rock flour proxies MS, LOI, and fine silt %. Light tan interval is interpreted to be the Tsoyowata ash and was reworked during transport, shifting up in the core stratigraphy.

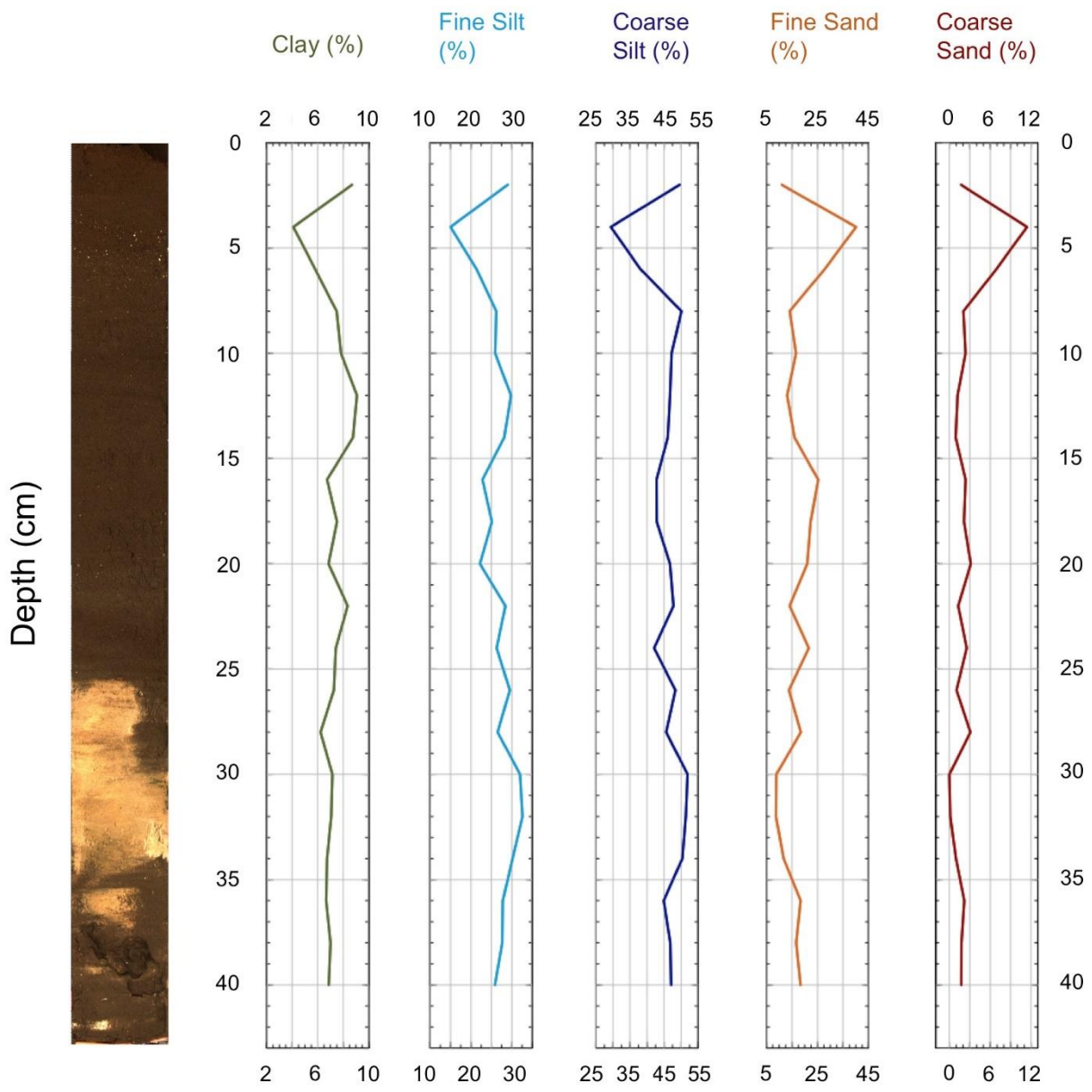

Figure 20. Sediment core LA16-G02 from Lake Aloha below the Price glaciers with grain size distribution of clastic sediments. Light tan interval is interpreted to be the Tsoyowata ash and was reworked during transport, shifting up in the core stratigraphy.

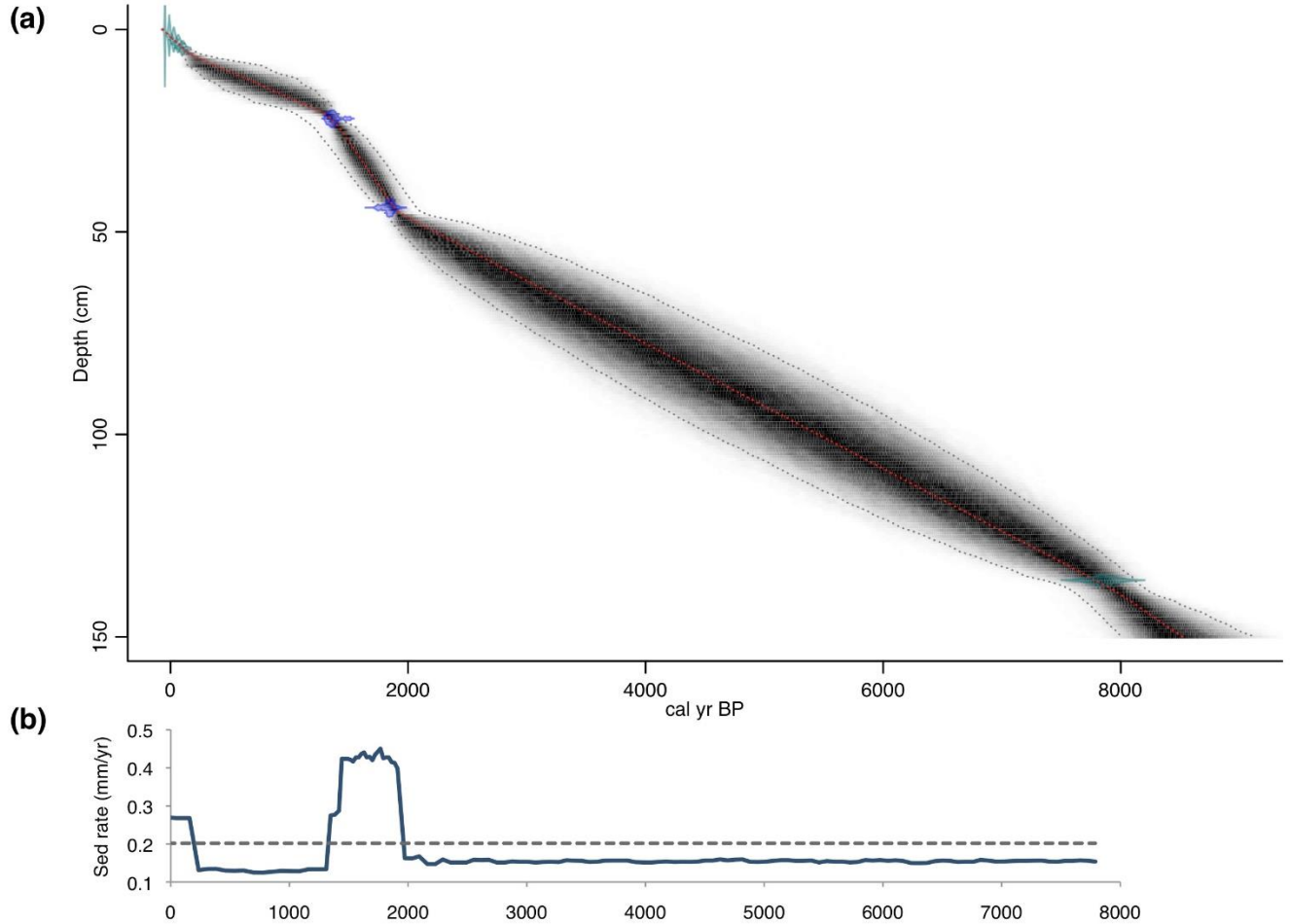

Figure 21. (a) Age-depth model for the Lyell composite core (pushes LL16-01-01, LL16-01-02, LL16-01-03, and LL16-01-04) produced using Bacon in r (Blaauw and Christen, 2011). Darker gray colors indicate more probable ages and are bound by the gray dashed lines that represent 95% confidence limits. Red dashed line displays the weighted mean age for each depth. Transparent blue symbols represent calibrated ^{14}C dates and green symbols indicate ^{210}Pb dates (first several cm depth) and tephra ages lower in the stratigraphy. (b) Sedimentation rate for each cm interval (blue line) and the overall average sedimentation rate (gray dashed line) plotted through time up to the oldest age constraint.

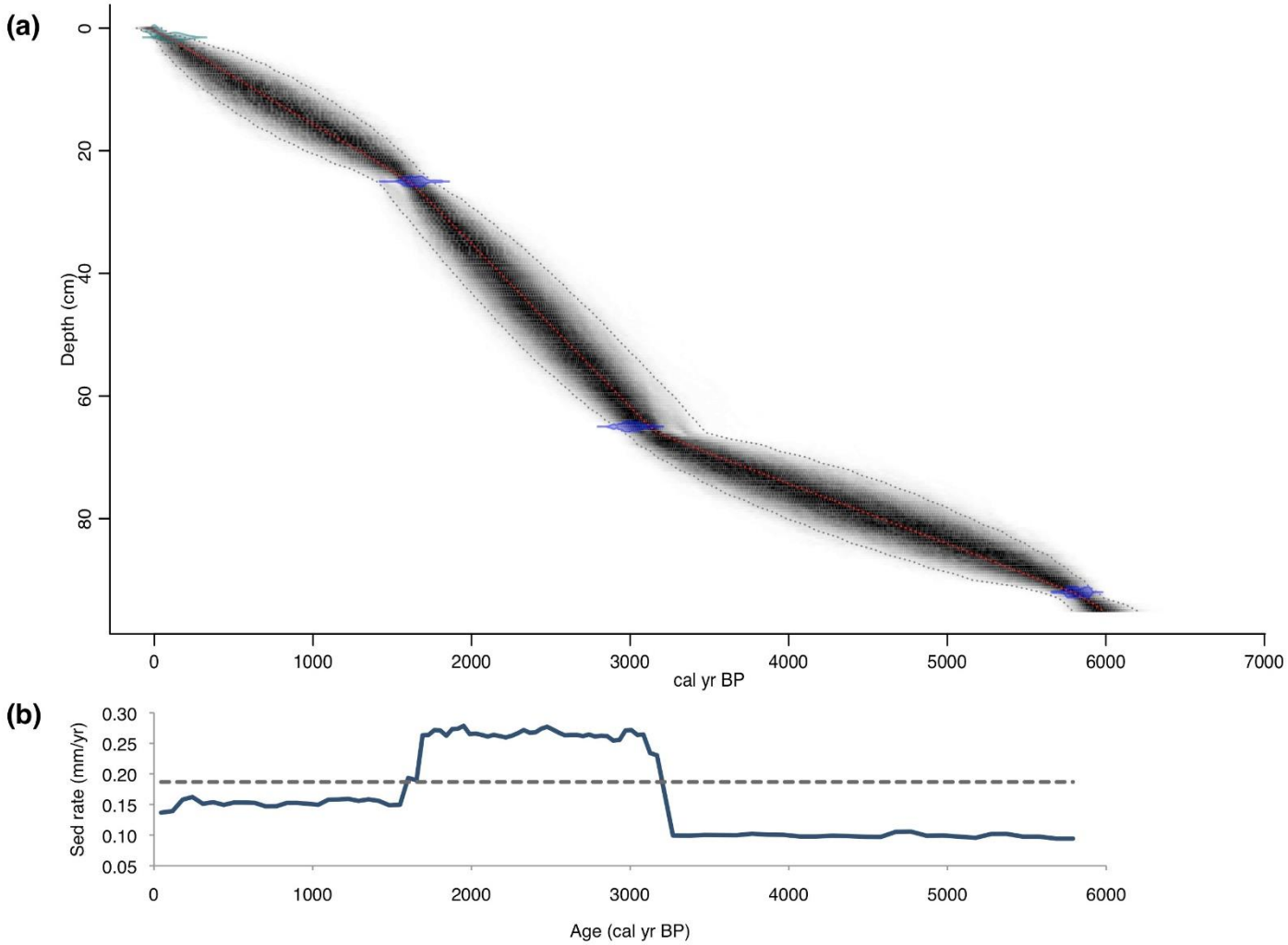

Figure 22. (a) Age-depth model for the Maclure core (LM16-01-01) produced using Bacon in r (Blaauw and Christen, 2011). Darker gray colors indicate more probable ages and are bound by the gray dashed lines that represent 95% confidence limits. Red dashed line displays the weighted mean age for each depth. Transparent blue symbols represent calibrated ^{14}C dates and green symbols indicate ^{210}Pb dates. (b) Sedimentation rate for each cm interval (blue line) and the overall average sedimentation rate (gray dashed line) plotted through time up to the oldest age constraint.

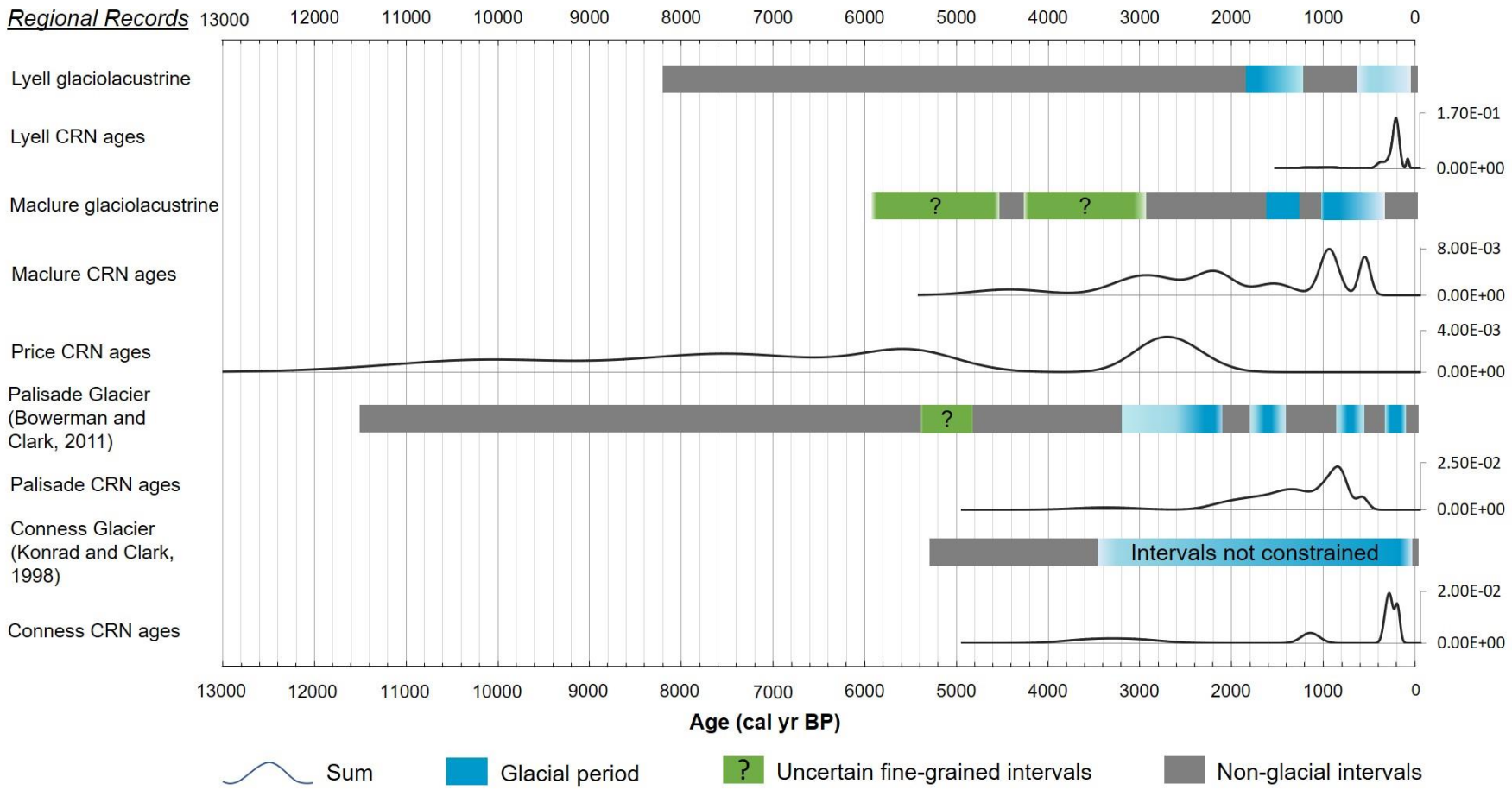

Figure 23. Plot of glacier fluctuations interpreted from glaciolucustrine records in the Sierra Nevada and CRN ages from each respective glacier displayed by the sum gaussian distributions with relative probability on the vertical axis (refer to Figures 3-5). Questions marks (?) indicate a possible, but uncertain glacial interval comprised of fine-grained sediment, but has not been interpreted as having a glacial origin. Blank space denotes there is no record available. Darker blue portions of glacial periods represent glacier maxima.